CHAPTER IV

DEPOLARIZATION ON EARTH-SPACE PATHS

4.1 INTRODUCTION

By using orthogonal polarizations, two independent information channels occupying the same RF frequency band can be transmitted over a single link. This technique is used in satellite communications systems to effectively increase the available spectrum. While the orthogonally-polarized-channels are completely isolated in theory, some degree of interference between them is inevitable, owing to less-than-theoretical performance of spacecraft and Earth station antennas, and depolarizing effects on the propagation path. The main sources of this depolarization at millimeter wave frequencies are hydrometer absorption and scattering in the troposphere.

4.1.1 Definition of Terms

Frequency reuse satellite communications systems utilize either orthogonal linear or circular polarization states. The orthogonal linear polarization (LP) states are normally referred to as vertical and horizontal, but except for Earth stations at the satellite's longitude, the polarization directions are rotated somewhat from the local vertical and horizontal references. The orthogonal circular states are left-hand and right-hand circular polarization (LHCP, RHCP), differing in the sense of rotation of the electric field vector. The "handedness" is defined as follows: a wave is RHCP if the sense of rotation of the field corresponds to the natural curl

of the fingers of the right hand when the right thumb is pointed along the propagation direction. Likewise for LHCP. Thus a RHCP wave coming out of the paper would have an electric field rotating counterclockwise.

A measure of the degree of interference between the two orthogonally-polarized channels is the crosspolarization discrimination (denoted XPD), defined as follows: Let E_{ij} be the magnitude of the electric field at the receiver that is transmitted in polarization state i and received in the orthogonal polarization state j (i,j=1,2). E_{11} and E_{22} denote the copolarized waves E_{12} and E_{21} refer to the crosspolarized waves. This is illustrated in Figure 4.1-1. XPD is the ratio (in dB) of the power in the copolarized wave to the power in the crosspolarized wave that was transmitted in the same polarization state.

$$XPD = 20 \log \frac{E_{11}}{E_{12}} \qquad (4.1\text{-}1)$$

If state "1" is RHCP and "2" is LHCP, for example, then the XPD is the ratio of the RHCP power to the LHCP power, given that only a RHCP wave was transmitted.

A closely related measure is the crosspolarization isolation (XPI), which compares the copolarized received power with the crosspolarized power that is received in the same polarization state:

$$XPI = 20 \log \frac{E_{11}}{E_{21}} \qquad (4.1\text{-}2)$$

Again letting the states "1" and "2" refer to RHCP and LHCP, the XPI compares the power in the RHCP received wave that was transmitted as RHCP to the power that was transmitted as LHCP. XPI is the

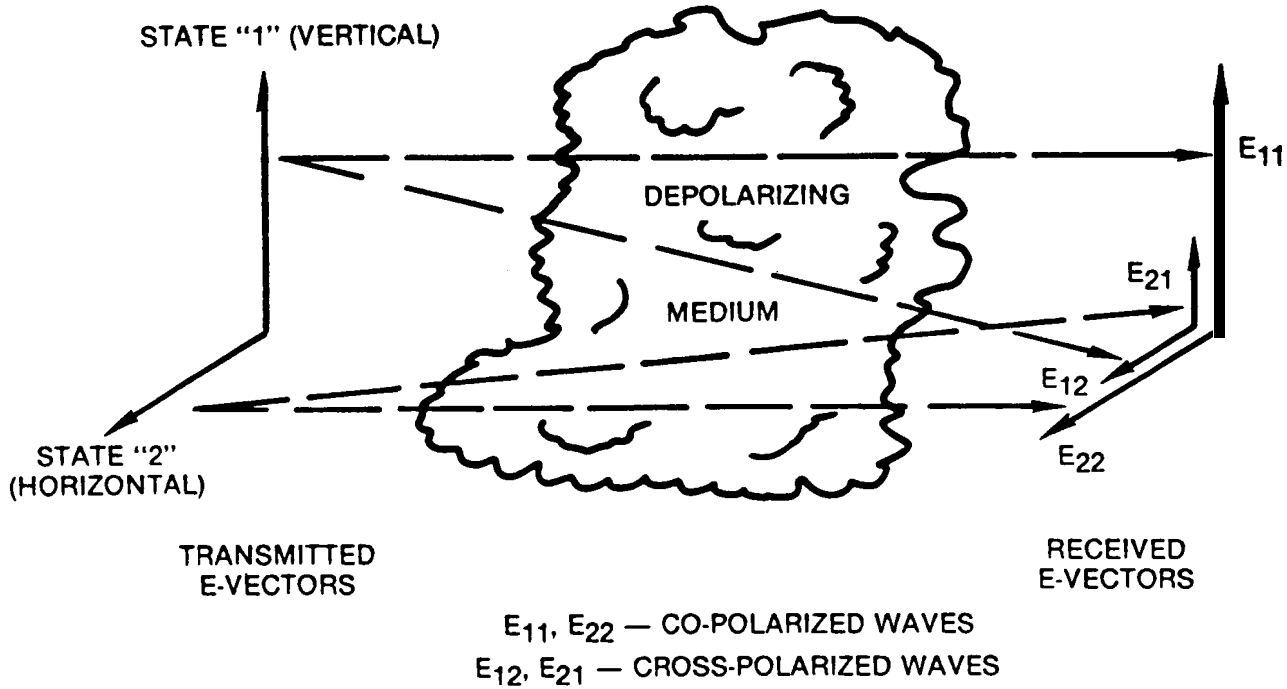

Figure 4.1-1. Definition of and Crosspolarization

parameter that is most meaningful to system engineers, since it directly gives the carrier-to-interference ratio in a received channel. However, XPD is the parameter that is most easily measured. It has been shown (Watson and Arbabi-1973) that XPI and XPD are the same if the hydrometers responsible for the depolarization have certain symmetry properties. The geometric models that have been used for raindrops and ice crystals have the necessary symmetry, so XPI = XPD in theory. In practice, it has been found that there is not a significant difference between XPI and XPD.

Another term used to describe depolarization, cross polarization ratio (CPR), is the reciprocal of XPD. Other parameters in use, e.g., crosstalk discrimination? crosspolarization distortion, depolarization ratio, crosspolarization level, usually reduce to XPD or XPI.

In the discussion that follows, it is often important to distinguish between polarization properties of a wave in space, and the parameters that we actually measure at the output of the receiver. We shall use XPD to describe the wave properties and a different term, Isolation (I) (after Stutzman-1977) to describe the receiver output. In general,

$$I = \frac{\text{copolarized channel output power}}{\text{crosspolarized channel output power}}$$

Isolation takes into account the performance of the receiver antenna, feed, and other components as well as the propagating "medium. When this performance is close to ideal, and/or the XPD of the wave is low (i.e. severe depolarization)? then I=XPD. This will be discussed in more detail later.

4.1.2 Hydrometer Sources of Depolarization

The major sources of depolarization on Earth-space paths are hydrometers, ionospheric Faraday rotation, and multipath. The

predominant source at millimeter wave frequencies is hydrometers, and rain is the hydrometer species that has the greatest effect."

4.1.2.1 Rain. To determine the attenuation due to rain, the raindrops are modelled as spheres of water suspended in space. Real raindrops are falling at their terminal velocity and, due to the complex aerodynamic and hydrostatic forces acting on them, they are in general not spherical. The very small drops (≥0.03 cm in diameter) are very nearly spherical, drops in the range of about 0.03 to 0.10 cm in diameter can be considered oblate spheroids, and drops with diameters larger than about 0.10 cm are asymmetric blobs with flat or concave bottoms (Pruppacher and Pitter-1971). Depolarization occurs because of this lack of spherical symmetry, along with the tendency for the drops to have a preferred orientation (i.e., top and bottom flattened). The effects of the rain-filled medium on a wave propagating through it are dependent on the orientation of the electric field vector with respect to the preferred drop orientation.

It is easy to picture the effect of the "flattened" raindrops on linearly polarized (LP) waves propagating horizontally: The fields of horizontal LP waves encounter more water, on the average, than do vertical LP wave fields, and so are subjected to more attenuation and phase shift. An LP wave at some arbitrary orientation, say 45° from the vertical, can be resolved into an equivalent set of component waves having horizontal and vertical polarization. After passing through the rain, the horizontal component has suffered a greater decreased in amplitude, so the polarization direction has been shifted toward the vertical. In addition, the differential phase shift between the components has caused the wave to become slightly elliptically polarized. These depolarizing effects of rain are described more rigorously later.

4.1.2.2 Ice Crystals. Most of the depolarizing effect of rain is produced by differential attenuation. Therefore rain depolarization and attenuation are fairly well correlated. Starting in 1975, when ATS-6 propagation experiments were well underway in Europe,

researchers were surprised to see occasions of severe depolarization that were completely uncorrelated with rain attenuation. The cause of this "anomalous" depolarization has since been identified as oriented ice crystals. Ice can occur at altitudes above the freezing level in cirrus clouds and at the tops of cumulonimbus clouds. When something causes the ice crystal symmetry axes to align themselves, it brings on a polarization-selective phase effect. We are now fairly certain that the electrostatic fields associated with electrically-active storms are at least one aligning force. This is consistent with the observed abrupt changes in XPD coincident with lightning flashes.

Ice depolarization has been theoretically modelled in a manner analogous to rain depolarization. For that purpose, the ice crystals are assumed to be either oblate or prolate ellipsoids, corresponding respectively to "plates" and "needles," which are two distinct types of crystals that are known to exist in clouds. The model is in good agreement with observations and explains the rapid changes in the phase of the crosspolarized waves that accompany lightning flashes.

4.1.2.3 Snow, Graupel and Hail. The anisotropy that is responsible for depolarization by rain and high-altitude ice crystals apparently also exists in snow. From S-band and Ku-band radar measurements, Hendry, et. al. (1976) have observed significant differential phase shifts between the right-and left-hand CP radar returns in moderate to heavy snow. The differential phase shift along the propagation path was found to vary between 0.16^{0} and 1.17° per km at 16.5 GHz, values comparable to that of moderate rainfall. Unlike rain, however, snow produces very little differential attenuation. The differential phase shift in snow should produce measurable depolarization on Earth-space paths, but little or no direct experimental evidence of this has been reported.

Graupel, or snow pellets, may also exhibit some anisotropy, and resulting depolarization. Hail particles, which have a rough

spherical symmetry, probably would not cause depolarization. (McCormick and Hendry-1977).

4.2 MATHEMATICAL FORMULATIONS FOR DEPOLARIZATION

This section presents the mathematical background required to discuss the effects of the propagation medium characteristics and antenna performance on signals in dual polarization Earth-space links. It should enable the system designer to properly interpret experimental data and assess system performance? considering both the medium's depolarizing effects on the wave and the wave's interaction with the antenna system. Most of this development is from Stutzman (1977).

4.2.1 Specifying the Polarization State of a Wave

In the most general case, the tip of the electric field vector of a plane electromagnetic wave traces out an ellipse in the plane perpendicular to the direction of propagation. The polarization state of the wave is given by specifying the shape and orientation of the ellipse, along with the sense of rotation of the field vector. Figure 4.2-1 shows the general polarization ellipse and defines the notation. The electric field vector $\vec{\mathcal{E}}(t)$ is the resultant of sinusoidal components $\mathcal{E}_x(t)$ and $\mathcal{E}_y(t)$ which have different amplitudes E_1 and E_2 and a phase difference δ:

$$\begin{aligned}\vec{\mathcal{E}}(t) &= \hat{x}\,\mathcal{E}_x(t) + \hat{y}\,\mathcal{E}_y(t) \\ &= \hat{x}\,E_1 \cos\omega t + \hat{y}\,E_2 \cos(\omega t + \delta)\end{aligned} \qquad (4.2\text{-}1)$$

where $\hat{x}$ and $\hat{y}$ are unit vectors in the x and y directions, respectively, ω is the radian frequency, and t is time. The polarization ellipse is fully described by the angle, τ, between the ellipse major axis and the x-axis, and the ratio of the major and minor axes of the ellipse. This ratio is the magnitude of an important parameter known as the axial ratio, and is the ratio of

the maximum to the minimum magnitude of the electric field vector. The axial ratio's sign is assigned to be positive if the vector rotation has a left-hand sense and negative for rotation with a right-hand sense: (See Figure 4.2-2.) Linearly polarized waves have an infinite axial ratio; circularly polarized waves have an axial ratio $r = \pm 1$, corresponding to LHCP and RHCP respectively,

It is convenient to define another parameter

$$\varepsilon = \cot^{-1} r \quad ; -45^\circ \leq \varepsilon \leq 45^\circ \tag{4.2-2}$$

The specifying parameters ε and τ are related to the quantities used to describe the fields earlier by

$$E = \frac{1}{2} \sin^{-1} (\sin 2\gamma \sin\delta) \tag{4.2-3}$$

$$T = \frac{1}{2} \tan^{-1} (\tan 2\gamma \cos\delta) \tag{4.2-4}$$

where

$$\gamma = \tan^{-1} \frac{\text{max y-component of } \vec{\mathcal{E}}}{\text{maxx-componentof } \vec{\mathcal{E}}} = \tan^{-1} (E_2/E_1) \tag{4.2-5}$$

There are other methods used to specify polarization state (Stutzman-1977). The Stokes parameter representation is a matrix formulation. The Poincare sphere is a mapping of polarization states into points on a unit sphere. The complex polarization factor is a single number specifying polarization state. All these various representations are directly relatable to the angles ε and τ, or δ and γ.

4.2.2 Wave-Antenna Interaction

The power available (P_R) at the output of an antenna illuminated by a uniformly polarized incident plane wave of flux density S is

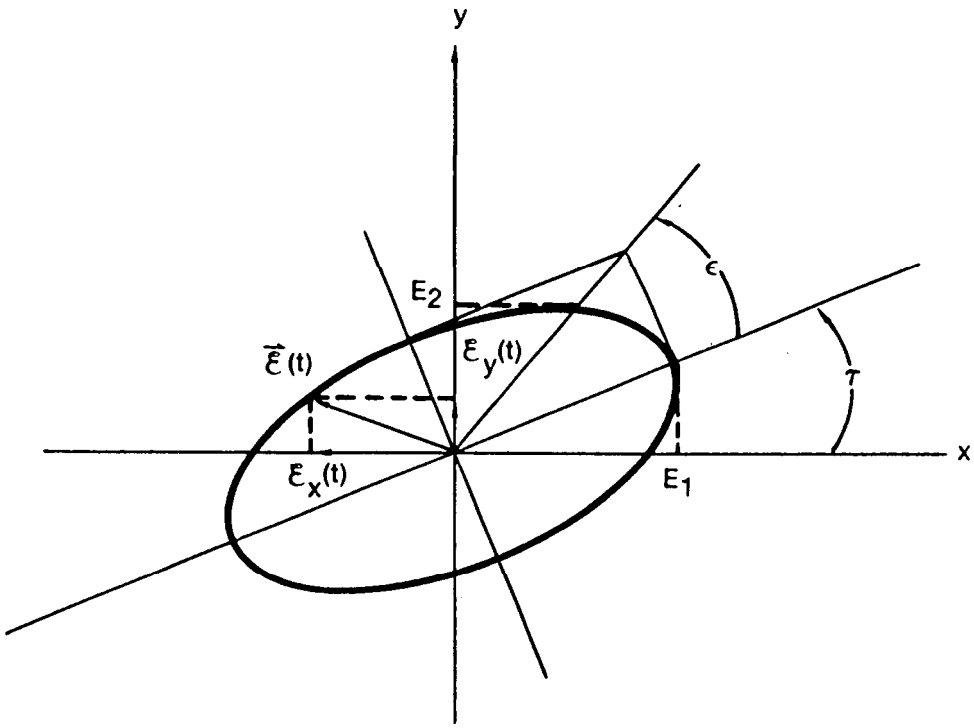

Figure 4.2-1. Polarization Ellipse

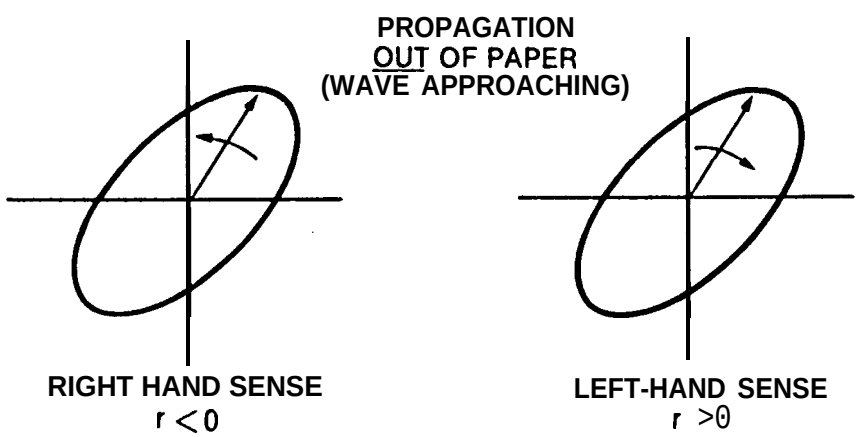

Figure 4.2-2. Definition of Sign of Axial Radio, r

$$P_R = S A_e m_p \qquad (4.2\text{-}6)$$

where A_e is the effective aperture of the antenna in the direction of the incident wave, and m_p is the polarization mismatch factor. This factor is a real number between zero and one that depends on the degree of match of the polarization state of the wave and the antenna. The polarization state of a receiving antenna is defined as the state of the wave that the same antenna would transmit, but with time reversed. (A time-reversal changes the direction of propagation of a wave but retains the sense of rotation and axial ratio.) A RHCP incident wave, for example, is perfectly matched to a RHCP antenna. This means the antenna absorbs the maximum amount of power from the wave, and $m_p = 1$. A RHCP antenna absorbs no power from a LHCP wave, and $m_p = 0$. The general expression m_p, assuming arbitrary elliptical polarization states of both the antenna and the wave, is

$$m_p(w,a) = \frac{1}{2} + \frac{4r_w r_a + (r_w^2 - 1)(r_a^2 - 1)\cos 2(\tau_a - \tau_w)}{2(r_w^2 + 1)(r_a^2 + 1)} \qquad (4.2\text{-}7)$$

where r_a = axial ratio of antenna

r_w = axial ratio of wave

τ_a = major axis angle of antenna

τ_w = major axis angle of wave

We consider some examples to confirm that (4.2-7) is plausible:

Antenna RHCP, Wave LHCP

$r_a = -1, \; r_w = +1$

$$m_p = 1/2 + \frac{4(1)(-1) + (1-1)(1-1)}{2(1+1)(1+1)} = 1/2 - 1/2 = 0$$

Antenna LP, Wave CP

$r_a = \infty, \quad r_w = 1$

By dividing the numerator and denominator of the second term of (4.2-7) by r^2_a, then taking the limit as $r \to \infty$, we find that $m_p = 1/2$, which is intuitively agreeable.

Antenna LP, Wave LP

$r_a = r_w = \infty$

Here we divide the numerator and denominator by $r^2_a r^2_w$ and pass to the limit, giving

$$m_p = 1/2 + 1/2 \cos 2(\tau_a - \tau_w) = \cos^2(\tau_a - \tau_w) \qquad (4.2\text{-}8)$$

This equals one when the orientation of the linear polarization axes of the antenna and wave are aligned $(\tau_a - \tau_w)$, and equals zero when the axes are orthogonal $(\tau_a - \tau_w = \pm 90^\circ)$

Antenna LP, Wave Elliptically Polarized

$r_a = \infty \qquad r_w = r$

Dividing through by r^2_a and taking the limit as before, we obtain

$$m_p = 1/2 + \frac{1/2\,(r^2-1)\cos 2(\tau_a - \tau_w)}{2(r^2+1)} \qquad (4\text{-}2.9)$$

Figure 4.2-3 is a polar plot of m_p versus the angle difference $\tau_a - \tau_w$, for $r = 1.5$ and 2.

Letting

$(m_p)_{max} = m_p$ for $\tau_a = \tau_w$ (aligned)

$(m_p)_{min} = m_p$ for $\tau_a = \tau_w + 90^\circ$ (orthogonal)

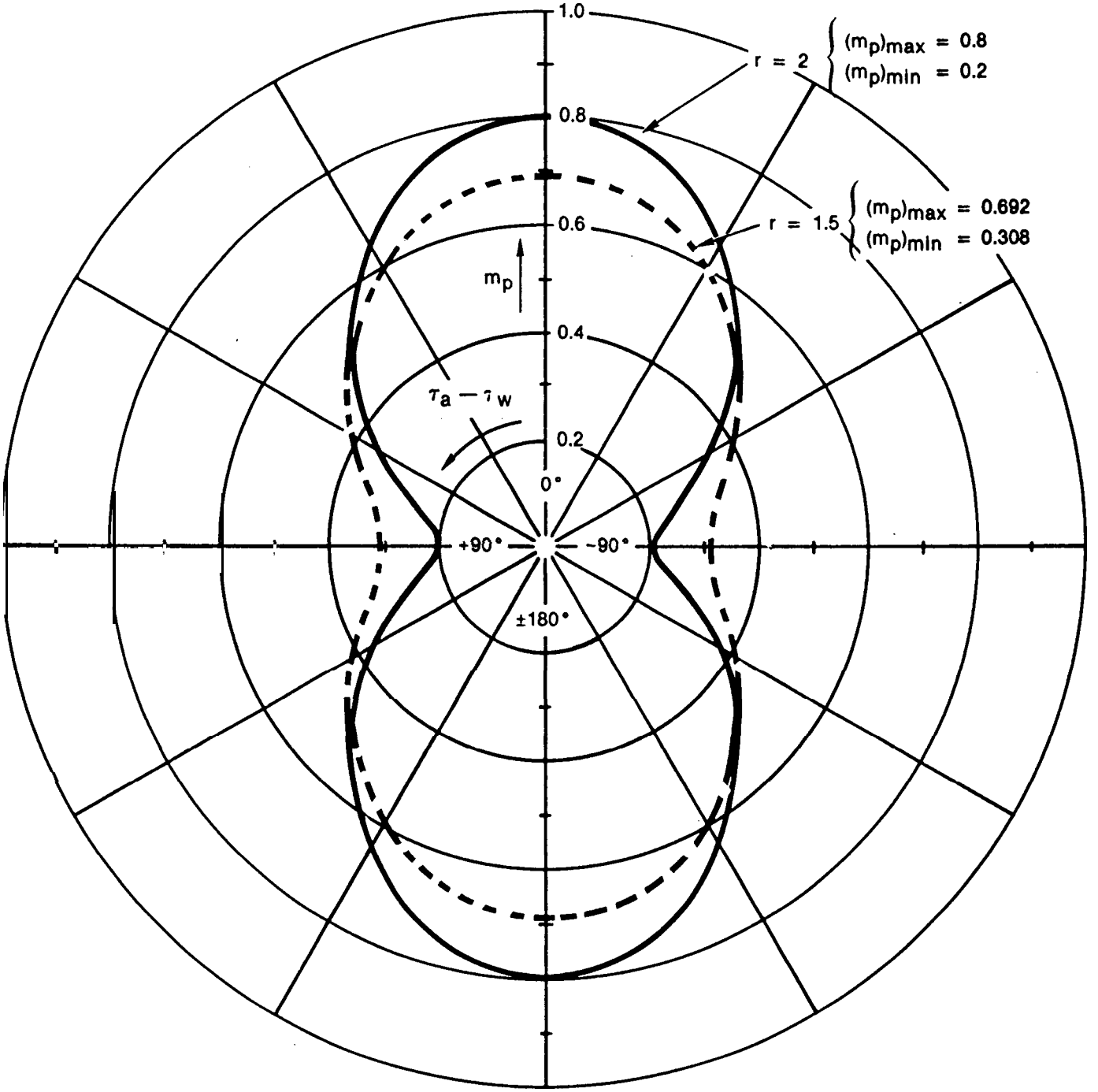

Figure 4.2-3. .Polarization Mismatch Factor m_p for LP Antenna and Elliptically Polarized Waves

Some algebra yields

$$r = \left[\frac{(m_p)_{max}}{(m_p)_{min}}\right]^{1/2} \qquad (4.2\text{-}10)$$

This is confirmed in Figure 4.2-3.

This formula suggests a technique for measuring the axial ratio and principal axis orientation of a received wave: The power received by a linearly polarized antenna (e.g., a dipole) is measured as the antenna axis is rotated through 180°. The ratio of the maximum to the minimum received power, assuming a perfect antenna, is then the square of the axial ratio of the wave, and the orientation of the wave's principal axis is just the antenna's orientation when maximum power is measured.

4.2.3 Cross Polarization Discrimination (XPD)

Having defined the polarization mismatch factor, we now present a more useful definition of XPD than that given earlier. Orthogonal polarization states are defined, in general, to have axial ratios that are equal in magnitude and opposite in sign (i.e., opposite in rotation *sense),* and have polarization ellipses with spatially orthogonal axes. Vertical/horizontal LP, and RHCP/LHCP are common examples of orthogonal states. The polarization mismatch factor for a wave with a given polarization state incident on an antenna that is matched to the orthogonal state is zero.

It is always possible to decompose a wave into two components with orthogonal polarization states. An arbitrary wave can be considered as being composed of a component with a polarization state matching the antenna, and a second component with the orthogonal state. The antenna extracts maximum power from the matched component, but completely rejects the orthogonal component. The polarization mismatch factor is then seen to be the proportion

of the total flux density impinging on the antenna that is being carried by the polarization-matched wave component. Denoting the received wave's polarization state by the index w', and the antenna's polarization state by w, the antenna output power is

$$P = SA_e m_p(w', w) \tag{4.2-11}$$

A second antenna with equal effective aperture A_e but with a polarization state w_o, that is exactly orthogonal to w, gives an output power

$$P_o = SA_e m_p(w', w_o) \tag{4.2-12}$$

The XPD is the ratio of the orthogonal components of the wave,

$$XPD = 10\log [m_p(w', w)/m_p(w', w_o)] \tag{4.2-13}$$

assuming that the "w" polarization state is the one the system is designed to maximize, or the copolarized state. The "w_0" state is designated as crosspolarized.

Suppose a LP wave is received, and the copolarized state (w) is designated as horizonally polarized. Let $\tau = \tau_w$, = the angle of the received wave with respect to horizonal. For this case,

$$m_p(w', w) = \cos^2\tau \tag{4.2-14}$$

$$m_p(w', w_o) = \sin\% \tag{4.2-15}$$

$$XPD = 10 \log (\cot^2\tau) \tag{4.2-16}$$

Assume an elliptically polarized wave is received with axial ratio $r_w' = r$, and copolar is designated as LHCP. For this case,

$$r_w = +1, \; r_{w_o} = -1 \tag{4.2-17}$$

$$m_p(w', w) = (1/2) \frac{(r+1)^2}{r^2+1} \tag{4.2-18}$$

$$m_p(w', w_o) = (1/2)\frac{(r-1)^2}{r^2+1} \qquad (4.2\text{-}19)$$

$$XPD = 20 \log [(r+1)/(r-1)] \qquad (4.2\text{-}20)$$

XPD is plotted versus r for the elliptically polarized case in Figure 4.2-4. An alternate "axial ratio," AR_{dB}, is shown in the figure. This is commonly used and is related to r by

$$ARdB = 20 \log |r| \qquad (4.2\text{-}21)$$

In terms of this parameter, XPD is closely approximated by

$$XPD \approx 24.8 - 20 \log (ARdB), \text{ for } ARdB < 10 \text{ dB} \qquad (4.2\text{-}22)$$

4.2.4 Effect of Non-Ideal Antenna Performance

The XPD describes the polarization characteristics of a received wave with respect to some "copolarized" reference. The true XPD could be measured with an ideal antenna, capable of being matched exactly to the co- and cross polarized state. Actual antennas are not ideal. They can be built with outputs that closely approximate the copolarized and crosspolarized components of the wave, but some degree of degradation is always present in their performance. Here we present a method of quantifying the polarization performance of the antenna and taking this performance into account in interpreting polarization measurements.

From this point on, the receive antenna polarization states that are close to the true co- and crosspolarized wave states will be distinguished from the true states by putting their names within quotation marks.

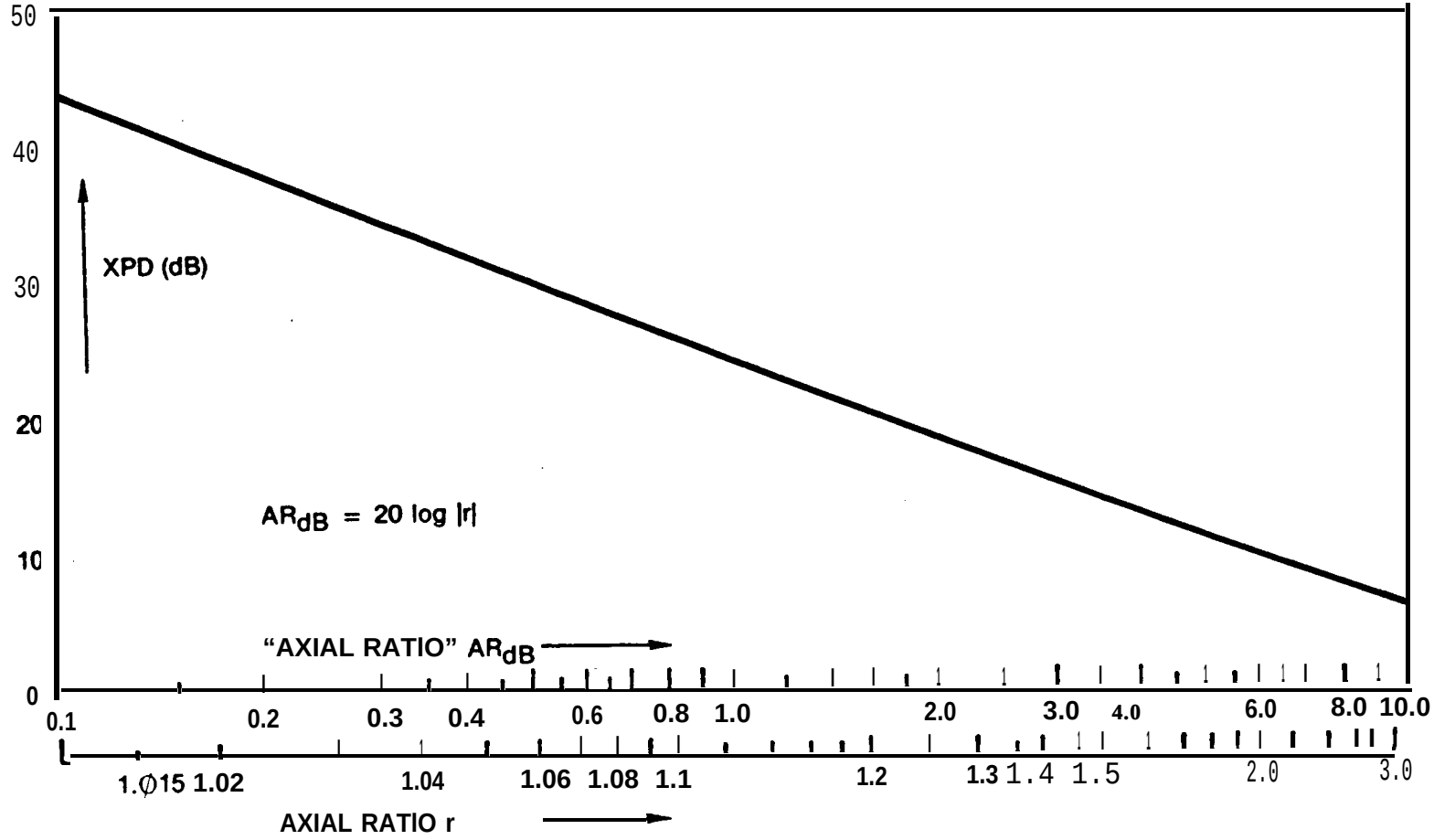

Figure 4.2-4. XPD VS. Axial Ratio of Elliptically Polarized Wave (LHCP is Copolarized)

Isolation, I, is defined as the ratio of the output power available at the antenna's "copolarized" port (P_c) to the output power at the "crosspolarized" port (P_x). The polarization states coupled to the "copolarized" and "crosspolarized" ports are a_c and a_x, respectively. Since the antenna is non-ideal, a_c and a_x are not necessarily orthogonal, and a_c does not necessarily correspond to the pure copolarized state. Denoting the state of the received wave as w' and the wave's power flux density as SW', we have from (4.2-11):

$$I = 10 \log \frac{P_c}{P_x} = 10 \log \frac{S_{w'} A_e m_p(w', a_c)}{S_{w'} A_e m_p(w', a_x)} \qquad (4.2\text{-}23)$$

$$= 10 \log \frac{m_p(w', a_c)}{m_p(w', a_x)}$$

It is useful to be capable of finding XPD in terms of I, which is measurable. The power available at the "copolarized" antenna port can be written in terms of the true copolarized and crosspolarized wave components, w and w_0.

$$P_c = A_e [S_w m_p(w, a_c) + S_{w_o} m_p(w_o, a_c)] \qquad (4.2\text{-}24)$$

Likewise for the "crosspolarized" power

$$P_x = A_e [S_w m_p(w, a_x) + S_{w_o} m_p(w_o, a_x)] \qquad (4.2\text{-}25)$$

S_w and S_{wo} are the power flux density in the true copolarized and crosspolarized states, respectively. Now we have

$$I = 10 \log \frac{S_w m_p(w, a_c) + S_{w_o} m_p(w_o, a_c)}{S_w m_p(w, a_x) + S_{w_o} m_p(w_o, a_x)}$$

$$= 10 \log \frac{(xpd)m_p(w,a_c) + m_p(w_o,a_c)}{(xpd)m_p(w,a_x) + m_p(w_o,a_x)} \qquad (4.2\text{-}26)$$

where $xpd = S_w/S_{w_o} = \log^{-1}(XPD/10)$

Since the "copolarized" state of the antenna is assumed to be well-matched to the true copolarized wave component,

$$m_p(w_o,a_c) << m_p(w,a_c)$$

So this term is negligible and

$$I = 10 \log \frac{m_p(w,a_c)}{m_p(w,a_x) + m_p(w_o,a_x)/(xpd)} \qquad (4.2\text{-}27)$$

Note that when the antenna is nearly ideal,

$$m_p(w,a_c) = 1,\ m_p(w_o,a_x) = 1,\ m_p(w,a_x) = 0$$

and so $I = XPD$. On the other hand, when the XPD is very high,

$$I = 10 \log [m_p(w,a_c)/m_p(w,a_x)]$$

which is a function of the antenna only. This implies that a given antenna can be used to measure XPD to a given accuracy up to a certain maximum XPD value which is determined by the antenna performance parameters.

For the CP case, the equation for I becomes

$$I = 10 \log \frac{\frac{1}{2} + \frac{r_c}{r_c^2 + 1}}{\frac{1}{2}(xpd^{-1} + 1) + \frac{r_x}{r_x^2 + 1}(xpd^{-1} - 1)} \qquad (4.2\text{-}29)$$

where r_c and r_x are the axial ratios of the antenna's "copolarized" and "crosspolarized" states, respectively. Figure 4.2-5 shows I versus XPD for various values of axial ratio AR_{dB}. The "copolarized" and "crosspolarized" axial ratios are made equal in the figures, but I is-actually nearly independent of r_x. The figure gives the amount of error to be expected when measuring XPD.

For the LP case, we obtain

$$I = \text{lolog} \frac{1 + Q_c \cos 2\tau_c}{(1 + xpd^{-1}) - (1-xpd^{-1})\, Q_x \cos\, 2(7X\text{-}90")} \qquad (4.2\text{-}30)$$

where $Q_{c,x} = (r_{c,x}^2 - 1)/(r_{c,x}^2 + 1)$

$\tau_{c,x}$ = antenna "copolarized", "crosspolarized" axis orientation angle

$r_{c,x}$ = antenna "copolarized", "crosspolarized" axial ratio

The copolarized wave axis is taken as the reference for the antenna axis orientation angles. Figures 4.2-6 and 4.2-7 show I versus XPD for various antenna axial ratios and axis misalignment angles. The first figure is for perfect axis alignment and varying axial ratio. As with the CP case, equal axial ratios for the "copolarized" and "crosspolarized" states were assumed, but isolation is practically independent of the "copolarized" axial ratio, r_c, when it is large (>20dB). Figure 4.2-7 shows the effect of axis misalignment for the AR_{dB}=30dB case. The antenna axes are assumed orthogonal, with $\tau_x = \tau_c$ -90°, but the isolation is not strongly dependent on τ_c for $\tau_c <$ 10°.

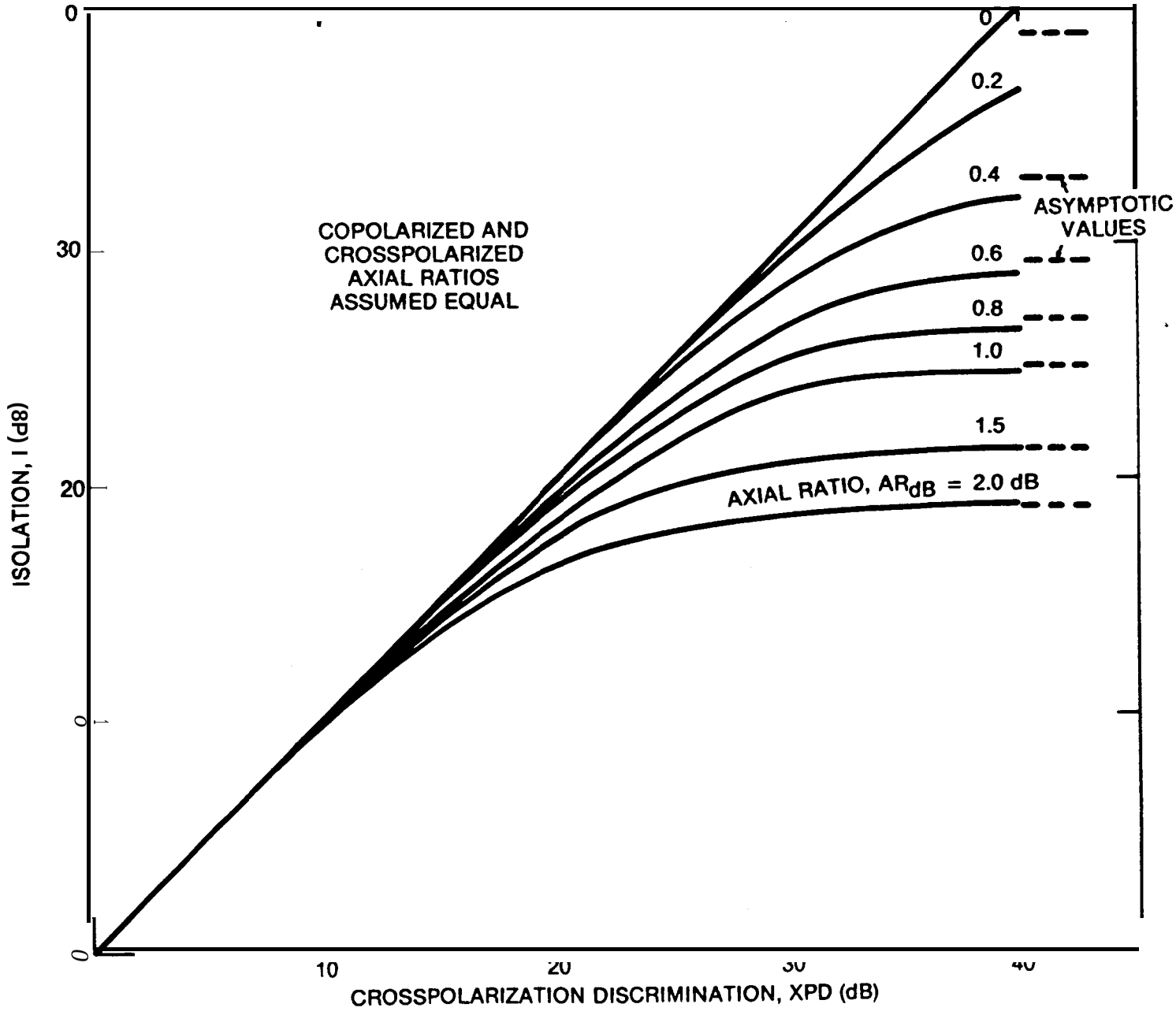

Figure 4.2-5. XPD and Antenna Axial Ratio - Circular Polarized Case

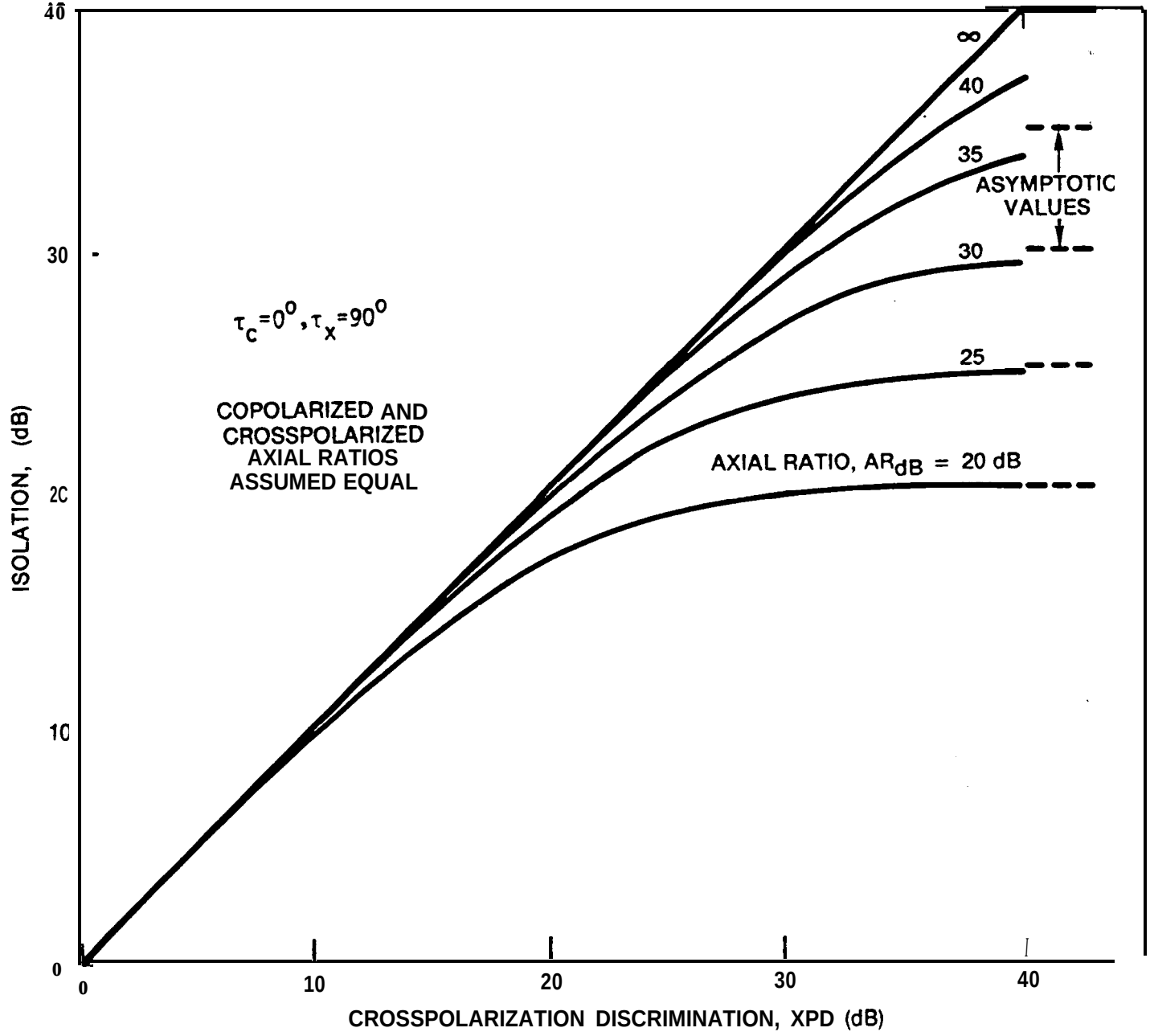

Figure **4.2-6.** Isolation vs. XPD and Antenna Axial Ratio - Linear Polarized Case, No Angle Misalignment

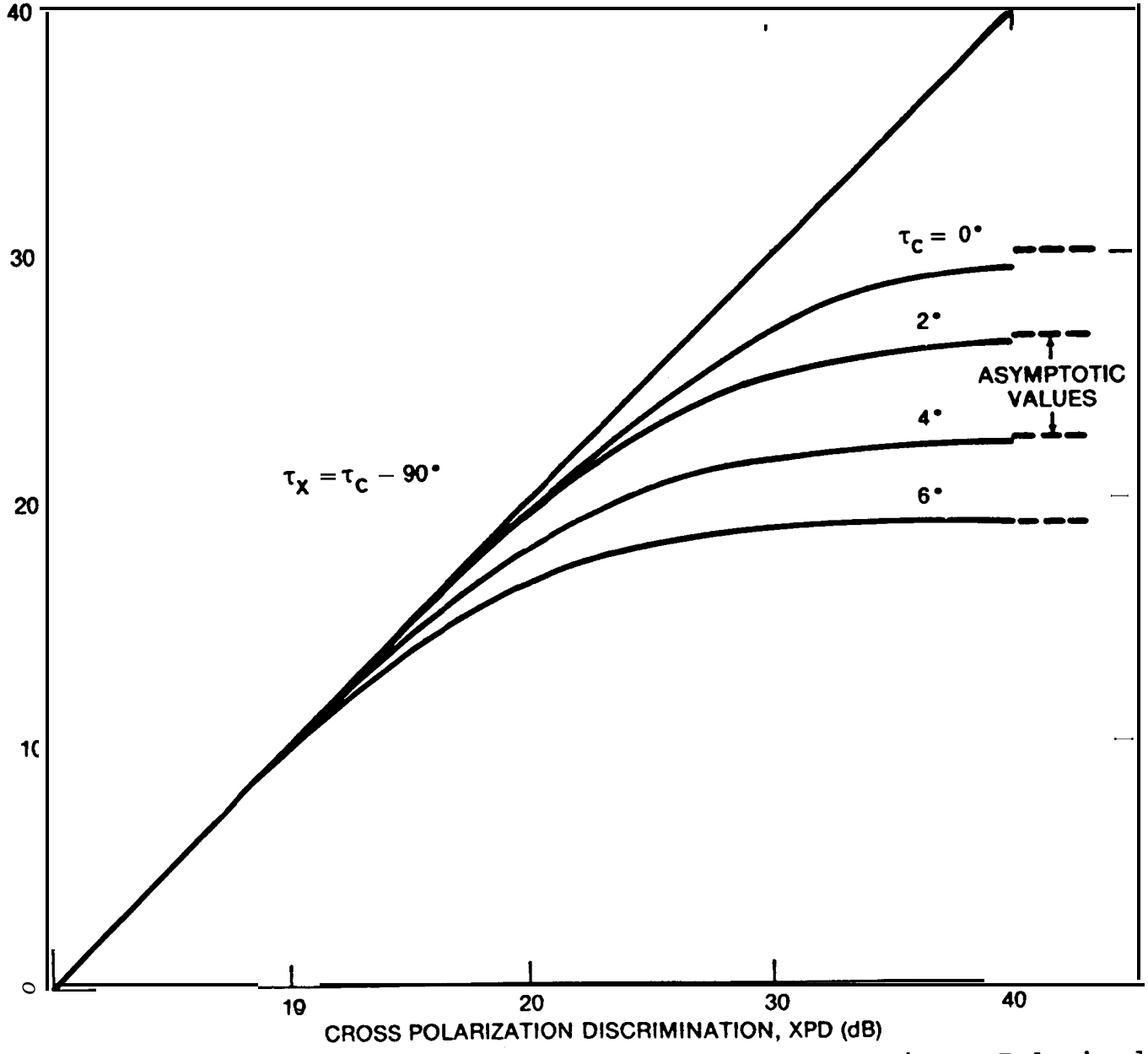

Figure 4.2-7. Isolation vs. XPD and Major Axis Misalignment - Linear Polarized Case, Axial Ratio, AR_{dB}=30dB

4.3 RAIN DEPOLARIZATION

4.3.1 Theory of Rain Depolarization

Rain depolarization can be modelled using the same techniques applied to rain attenuation. The essential difference is that in examining depolarization, the raindrops are assumed to be oblate spheroids. The attenuation analysis assumed that the raindrops were spherical. Figure 4.3-1 shows the geometry for a dual LP wave incident on an oblate spheroidal raindrop. The raindrop is at an arbitrary orientation with respect to the direction of propagation of the wave. The orientation is specified by the angle q, between the propagation vector and the raindrop's symmetry axis. The plane containing a will be referred to as the plane of incidence.

E_x and E_y are electric field vectors of two orthogonal LP waves. They are in a plane normal to the propagation vector, and each one can be resolved into two components: a component in the plane of incidence, and a component normal to it. Parallel to these components, we define two symmetry axes, labeled I and II in the figure. The projection of the raindrop into the plane containing the electric field vectors is an ellipse, and axes I and II are its minor and major axes, respectively. Figure 4.3-2 shows this ellipse and how the electric fields are resolved into their "I" and "II" components.

The total electric field magnitudes in the I and II directions (E_I and E_{II}) are given by

$$\begin{bmatrix} E_I \\ E_{II} \end{bmatrix} = \begin{bmatrix} \cos\theta & -\sin\theta \\ \sin\theta & \cos\theta \end{bmatrix} \begin{bmatrix} E_x \\ E_y \end{bmatrix} = R \begin{bmatrix} E_{x'} \\ E_{y'} \end{bmatrix} \qquad (4.3\text{-}1)$$

where θ, the canting angle, is the angle between the x and I axes.

Now consider a region of space containing many identical raindrops with the same orientation distributed throughout it. According to scattering theory, the effect of many scatterers along

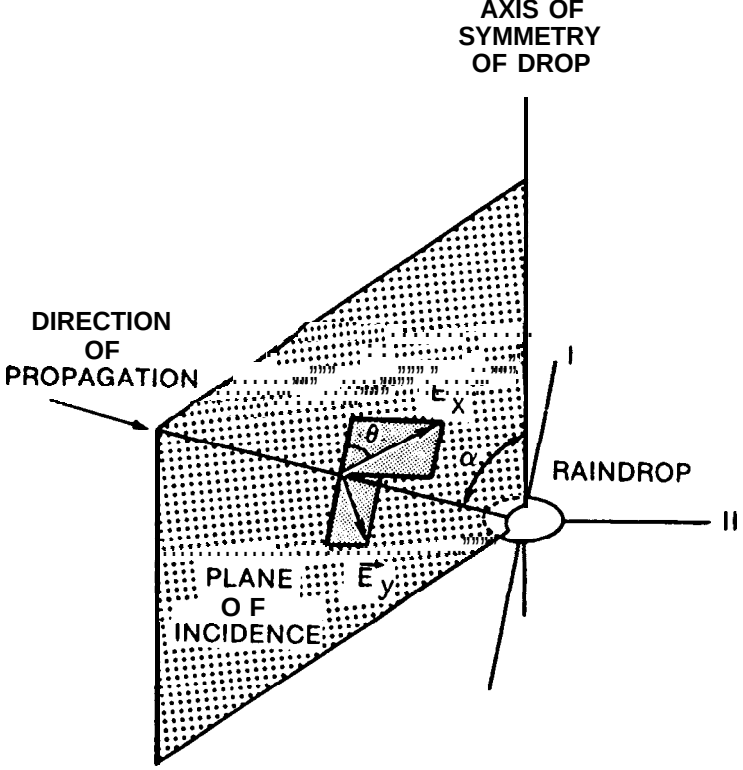

Figure 4.3-1. Geometry for Rain Depolarization Analysis

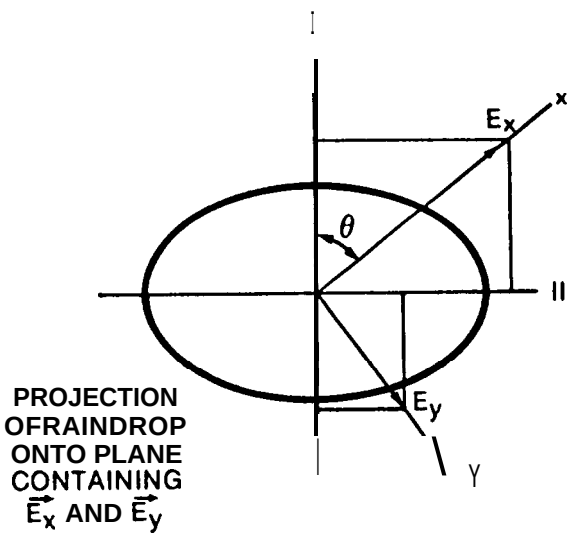

Figure 4.3-2. Resolution of Electric Fields into I and II Components

the propagation path of a wave is to multiply the electric field vector by a transmission coefficient of the form

$$T = \exp[-(a-j\phi)L] \qquad (4.3\text{-}2)$$

where L is the path length through the scattering region. The a term of the exponent produces attenuation of the wave, and ϕ produces a phase lag. This phase lag is in addition to the normal free-space phase retardation of the fields. Instead of a and ϕ, which have units of nepers per unit length and radians per unit length, respectively, the more useful parameters, A and $\underline{\Phi}$, are normally used:

A = specific attenuation of power flux density of wave, in dB/km.

$= 20(\log_{10}e)a = 8.686\ a$

$\underline{\Phi}$ = specific phase lag of wave, in degrees/km.

$= (180/n)\ \phi$

A region filled with oblate spheriodal raindrops must be characterized by two transmission coefficients: T_I, applied to the "I" component of the electric field, and T_{II}, applied to the "II" component. Denoting the fields of the wave incident on the scattering region by a subscript i, and the fields of the wave exiting the region by s (for scattered), we can write

$$\begin{bmatrix} E_{Is} \\ E_{IIs} \end{bmatrix} = \begin{bmatrix} T_I & 0 \\ 0 & T_{II} \end{bmatrix} \begin{bmatrix} E_{Ii} \\ E_{IIi} \end{bmatrix} = [T] \begin{bmatrix} E_{Ii} \\ E_{IIi} \end{bmatrix} \qquad (4.3\text{-}3)$$

Now the coordinate rotation R, defined above, can be applied to get an equation for the effect of the scattering region on the field vectors in the x and y directions.

$$\begin{bmatrix} E_{xs} \\ E_{ys} \end{bmatrix} = R^{-1} T R \begin{bmatrix} E_{xi} \\ E_{yi} \end{bmatrix} = T' \begin{bmatrix} E_{xi} \\ E_{yi} \end{bmatrix} \qquad (4.3\text{-}4)$$

Figure 4.3-3 shows how the three component transformations are successively applied to produce T′ . The overall transformation matrix T′ can be evaluated to yield

$$T' = \begin{bmatrix} t_{xx} & t_{xy} \\ t_{yx} & t_{yy} \end{bmatrix}$$

$$\begin{aligned} t_{xx} &= T_{\parallel} \cos^2\theta + T_{\perp} \sin^2\theta \\ t_{yy} &= T_{\parallel} \sin^2\theta + T_{\perp} \cos^2\theta \\ t_{xy} &= t_{yx} = \frac{1}{2}(T_{\perp} - T_{\parallel}) \sin 2\theta \end{aligned} \qquad (4.3\text{-}5)$$

Chu (1974) gives expressions for these parameters in terms of the As and Φs.

Calling the LP wave polarized *in* the x direction the copolarized wave, we can now obtain expressions for the XPD:

$$\begin{aligned} XPD_x &= 10 \log \frac{|E_{xs}|^2}{|E_{ys}|^2} \quad \text{with } E_{yi} = 0 \\ &= 10 \log \frac{|t_{xx}|^2}{|t_{yx}|^2} \\ &= 20 \log \frac{1 + \gamma \tan^2\theta}{(\gamma - 1) \tan\theta} \end{aligned} \qquad (4.3\text{-}6)$$

where

$$\gamma = T_{\parallel}/T_{\perp} = \exp\left[-(a_{\parallel} - a_{\perp})L + j(\phi_{\parallel} - \phi_{\perp})L\right]$$

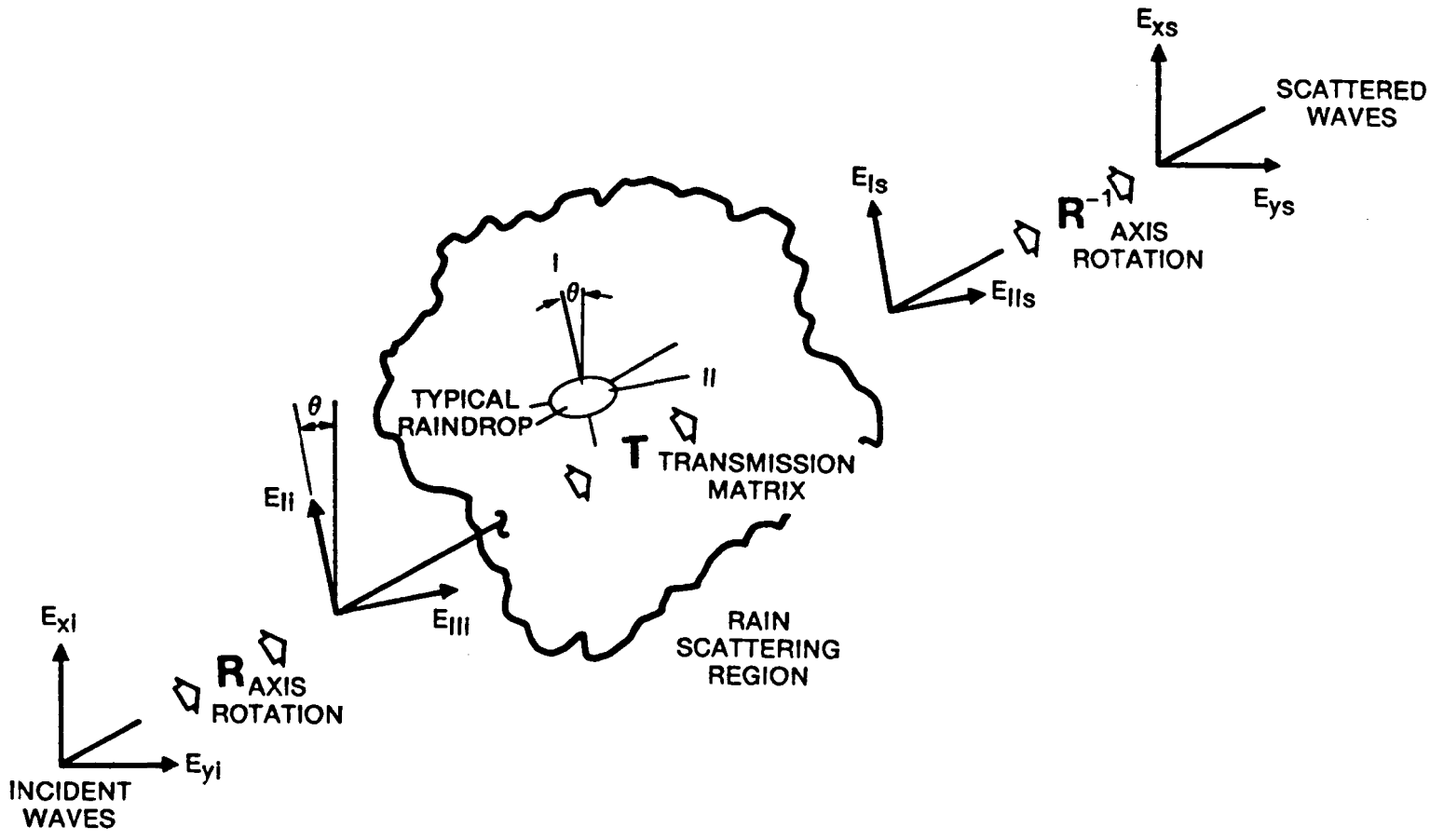

Figure 4.3-3. Components of Overall Transformation matrix T' Describing Rain Depolarization

Or, calling the y- direction the copolarized state,

$$XPD_y = 10\log \frac{|E_{ys}|^2}{|E_{xs}|^2} \quad \text{with } E_{xi} = 0$$

$$= 10 \log \frac{|t_{yy}|^2}{|t_{xy}|^2} \qquad (4.3\text{-}7)$$

$$= 20\log \frac{\gamma + \tan^2\theta}{(\gamma-1)\tan\theta}$$

For the case of circular polarization, Chu (1974) shows

$$XPD_c = 10 \log (|t_{xx}/t_{yx}|^2)_{\theta=45^\circ} = 20109 \frac{\gamma + 1}{\gamma - 1} \qquad (4.3\text{-}8)$$

which is independent of the sense of rotation of the copolarized wave.

Thus far, we have assumed that all raindrops are of equal size and have the same orientation. The model must account for the distribution of sizes and shapes of raindrops and the distribution of angles θ and a that are present in the rain along the path. Scattering theory allows for this. The scattering effect of a single raindrop is determined as a function of some parameter (like size), then the distribution of that parameter over the population of raindrops is used in calculating the transmission coefficients. The transmission coefficients (more exactly, the specific attenuations and phase lags, A and Φ) have been calculated in this manner as a function of rain rate by several authors. The first calculations (Chu-1974, Watson and Arbabi-1973a) used oblate spheroidal raindrops. The drops were assumed to be distributed

be distributed according to the well-known Laws and Parsons distribution, and to have eccentricities that were directly related to their sizes, with the largest drops being the most deformed. Later work has considered the more realistic Pruppacher-Pitter (1971) drop shapes (Oguchi-1977). Figure 4.3-4 (from Morrison, et al -1973) is an example of the results of these calculations. These curves give the difference in the specific attenuation and phase between the I and II axes. The angle between the direction of propagation and the raindrop symmetry axis, a , is a parameter, and the canting angle, θ, is set to 25°. The differential attenuation and phase are of most interest because they actually determine XPD. As can be seen from the curves, the worst case for differential attenuation and phase corresponds to a = 90°. This agrees with intuition, since the projection ellipse of the drop onto the plane containing the field vectors has the greatest eccentricity for that case. For values of a different from 90°, Chu (1974) shows that the following approximation is quite accurate:.

$$A_{II}-A_{I} = \sin^2\alpha \, (A_{II}-A_{I})_{\alpha=90°} \qquad (4.3\text{-}9)$$

$$\Phi_{II}-\Phi_{I} = \sin^2\alpha \, (\Phi_{II}-\Phi_{I})_{\alpha=90°}$$

Accounting for the distribution of a and θ is more difficult than doing so for drop size and shape. We have little information about the distribution of the orientation of raindrops. It is expected that wind and wind gusts produce an appreciable spatial correlation in the orientation. In the absence of wind, a fairly symmetric distribution about the vertical would be expected.

The a component of drop orientation is usually considered to be equal to a constant 90° for line-of-sight (horizontal) paths and the complement of the elevation angle for satellite (oblique) paths. The effect of α on XPD is apparently so small compared with the canting angle dependence that allowing for a distribution of α is not worthwhile.

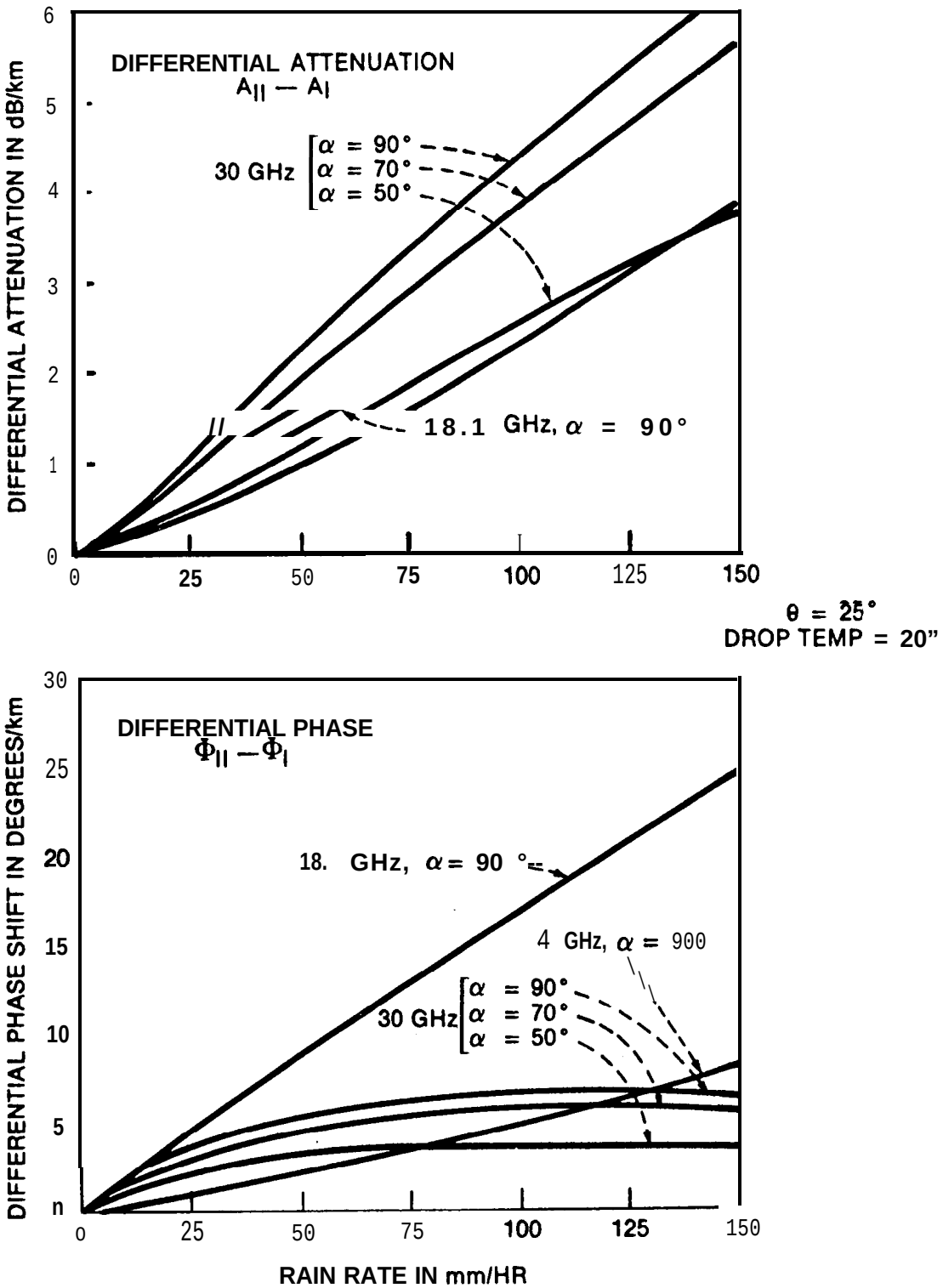

Figure 4.3-4. Differential Attenuation and Phase for Rain, From Morrison, et. al. (1973)

The canting angle distribution, as it affects XPD, has been studied extensively. Thomas (1971) presents an experimentally determined canting angle distribution and derives an "average" angle of 15°. He further notes that the crosspolarizing effects of canting angles of positive and negative sense tend to cancel, so the overall effect is proportional to the excess of one sense over the other. Based on some experimental evidence, he chooses 25% as the worst case imbalance of canting angle sense. The predicted worst case XPD, then, is roughly that produced by 25% of the raindrops at a lS° canting angle. Chu (1974) uses similar reasoning, but gives evidence that the mean canting angle is about 25°, and that the effective angle sense imbalance is about 14%. Watson and Arbabi (1973b) calculate XPD versus rain rate at 11 GHz assuming a Gaussian canting angle distribution with a non-zero mean value, and uncorrelated drop orientations. The results were nearly the same as those assuming a fixed canting angle equal to the mean value.

Distributions of both a and θ can be accounted for by the following transformation (Oguchi-1977). :

$$\begin{bmatrix} a_{I} - j\phi_{I} \\ a_{II} - j\phi_{II} \end{bmatrix} = \begin{vmatrix} 1 + m_{\theta}m_{\alpha} & 1 - m_{\theta}m_{\alpha} \\ 1 - m_{\theta}m_{\alpha} & 1 + m_{\theta}m_{\alpha} \end{vmatrix} \begin{vmatrix} a_{I}' - j\phi_{I}' \\ a_{II}' - j\phi_{II}' \end{vmatrix} \qquad 4.3\text{-}10)$$

where the unprimed a's and ø's are effective attenuation and phase constants and the primed ones correspond to α=90°. The canting angles and incidence angles are assumed to be randomly distributed with means θ and a variances δ_{θ}^2 and δ^2_{α} . The transformation parameters, assuming Gaussian distributions, are

$$m_{\theta} = \exp\left(-2\delta_{\theta}^2\right) \qquad (4.3\text{-}11)$$

$$m_{\theta} = \exp\left(-20_{\theta}^{2}\right)$$

$$m_{\alpha} = \frac{1}{2}\left[1 + \exp\left(-20_{\theta}^{2}\right)\right] \sin 2\bar{\alpha}$$

where σ_θ and σ_α are in radians. The effective canting angle used in the formulas for XPD, etc. is θ. Substituting the effective attenuation and phase constants a, ϕ into the formula for XPD (4.3-6), making the small argument approximation

$$\begin{aligned} Y &= \exp\left[-(a_{II}' - a_I')L + j(\phi_{II}' - \phi_I')L\right] \\ &\approx 1 - (a_{II}' - a_I')L + j(\phi_{II}' - \phi_I')L \end{aligned} \tag{4.3-12}$$

and making further approximations based on the known values of the a's and ϕ's, we arrive at

$$XPD \approx -20 \log \left\{ \frac{1}{2} m_\theta m_\alpha L[(\Delta a')^2 + (\phi')^2]^{1/2} \sin 2\bar{\theta} \right\} \tag{4.3.13}$$

where'

$$A a' = a_{II}' - a_I'$$

$$\Delta\phi' = \phi_{II}' - \phi_I'$$

This is good approximation for frequencies in the 4-50 GHz range and rain rates less then 150 mm/hr. If, in addition, we neglect the effect of the distribution of a and assume that the drops are oriented horizontally in the plane of incidence, as do Nowland, et.al. (1979), we can write

$$\begin{aligned} \sigma_\alpha^2 &\ll 1 \\ \bar{\alpha} &\approx 90° - \varepsilon \end{aligned} \tag{4.3-14}$$

where & is the antenna elevation angle. This implies

$$m_\alpha = \cos^2\varepsilon \tag{4.3-15}$$

which further simplifies the approximation for XPD. The result is

$$XPD \approx -20 \log \left| \frac{1}{2} m_\theta L |\Delta k'| \cos^2 \varepsilon \sin 2\bar{\theta} \right| \qquad (4.3-16)$$

with

$$|\Delta k'| = [(\Delta a')^2 + (\Delta \phi')^2]^{1/2}$$

4.3.2 Relationship between Depolarization and Attenuation due to Rain

An empirical relation has been observed between the exceedance statistics for attenuation and those for XPD on the same path. The relation is

$$XPD \approx \tilde{a} - \tilde{b} \log(CPA) \qquad (4.3-17)$$

where XPD is the value of cross-polarization discrimination not exceeded for a given percentage of the time, and CPA is the copolarized attenuation value in decibels, exceeded for the same percentage of the time. The empirical constant $\tilde{a}$ is typically found to be in the 30-50 dB range and $\tilde{b}$ is usually around 20. We present below the theoretical basis supporting this relation, and examine some of the experimental evidence for it.

Referring back to Section 4.3.1, we can obtain an expression for attenuation of the copolarized wave in a manner similar to finding the XPD. The copolarized attenuation, assuming a LP incident wave oriented in the x-direction, is given by

$$\begin{aligned} CPA &= -10 \log \frac{|E_{xs}|^2}{|E_{xi}|^2} \text{ with } E_{yi} = 0 \\ &= -10 \log |t_{xx}|^2 \\ &= -20 \log |T_I \cos^2\theta + T_{II} \sin^2\theta| \\ &= -20 \log |T_I [1 + (e^{-(\Delta a - j\Delta\phi)} - 1) \sin^2\theta]| \end{aligned} \qquad (4.3-18)$$

where Aa and $\Delta\phi$ are defined under equation (4.3-13). Using the small argument approximation (4.3-12) we can obtain

$$CPA, \approx -20 \log [\exp(-a_I L \cos^2\theta - a_{II} L \sin\%)]$$

$$= (A_I \cos^2\theta + A_{II} \sin^2\theta) L \qquad (4.3\text{-}19)$$

The same expression, with 1 and II subscripts interchanged, is found for CPA_y . Note that the above expression applies only when all the raindrops have the same orientation. Averaging over distributions of orientation angles a and 6, as was done earlier to find the XPD, we obtain

$$CPA_x = \frac{1}{2}[(A_I' + A_{II}') + m_\theta m_\alpha (A_I' - A_{II}') \cos 2\bar{\theta}]L \qquad (4.3\text{-}20)$$

where A_I' and A_{II}' are the attenuation coefficients, in dB/km, for a $= 90°$. Again assuming as before, that the raindrops are not distributed in a, and that a = $90^o - \varepsilon$,

$$CPA, = \frac{1}{2}[(A_I' + A_{II}') + m_\theta (A_I' - A_{II}') \cos^2\varepsilon \cos 2\bar{\theta}]L \qquad (4.3\text{-}21)$$

CPA_y is the same except that the sign of the second term is minus.

To relate XPD and CPA, we assume that the CPA, the attenuation coefficients A_I and A_{II}, the magnitude of the differential propagation constant, and the effective path length all bear a power law relation to the effective rain rate, R (Nowland, et al-1977):

$$CPA = a_0 R^{b_0} L \qquad (4.3\text{-}22a)$$

$$A_{I'} = a_1 R^{b_1} \qquad (4.3\text{-}22b')$$

$$A_{II'} = a_2 R^{b_2} \qquad (4.3\text{-}22c)$$

$$L = u R^{v} \qquad (4.3\text{-}22d)$$

$$|\Delta k| = c R^{d} \qquad (4.3\text{-}22e),$$

Substituting (4.3-22a-c) into (4.3-21) gives approximate expressions for a_0 and b_0 in terms of a_1, a_2, b_1 and b_2, which can be determined by regression fitting to the calculated propagation constants. The parameters u, v, c and d can also be determined by regression fitting to theoretical or empirical relations.

Substituting (4.3-22d) and (4.3-22e) into the formula for XPD, (4.3-16), gives XPD in terms of R and regression parameters. Likewise, using (4.3-22d) in (4.3-22a) gives CPA in terms of R and regression parameters. Elmininating R then relates XPD and CPA:

$$XPD \cong \tilde{a} - \tilde{b} \log CPA \qquad (4.3\text{-}23)$$

with

$$\tilde{a} = 20 \left(\frac{d+v}{b_0+v}\right) \log(a_0 u) - 20 \log\left(\frac{1}{2} c\, u\, m_\theta \cos^2\xi \sin 2\bar{\theta}\right)$$

$$\tilde{b} = 20\left(\frac{d+v}{b_0+v}\right) \qquad (4.3\text{-}24)$$

In the 11-14 GHz range, $b_0 = d$, which simplifies the formulas:

$$\tilde{a} \cong -20 \log\left(\frac{1}{2a_0} c\, m_\theta \cos^2\xi \sin 2\bar{\theta}\right)$$

$$\tilde{b} \cong 20 \qquad (4.3\text{-}25)$$

Throughout the preceding development, linear polarization in the x direction was assumed. For LP waves in the y- direction, the 1

and 2 subscripts in the formulas for a_o and b_o are reversed. For CP waves, 8 is set to 45°, which gives the lowest value of XPD.

The CCIR developed a provisional formula based on the above analysis, which provided a simplified form to allow for the prediction of XPD for a given percentage of the time. The CCIR formula was first presented in CCIR Report 564-1, (CCIR-1978), and later updated and modified in Report 564-3, (CCIR-1986). The CCIR formula essentially sets

$$d \cong b_o$$

$$\frac{cm_\theta}{2a_0} \approx [f(GHz)]^{-3/2} \qquad (4.3\text{-}26)$$

$\tilde{\theta} \approx \tau$ = polarization tilt angle with respect to horizontal

to arrive at the "CCIR Approximation"

$$XPD = 30 \log[f(GHz)] - 40 \log(\cos \tau) - 10 \log[1 - .484(1 + \cos(4\tau))]$$
$$- 20 \log (CPA) + .0052\sigma_\phi^2 \qquad (4.3\text{-}27)$$

where σ_ϕ is the effective standard deviation of the raindrop canting angle distribution, expressed in degrees. [The CCIR prediction procedure is described in detail in Chapter VI, prediction Techniques.]

The "exact" evaluation of the a and b coefficients requires first finding a_1, b_1, a_2, b_2, c and d by regression fitting to the parameters A_I, A_{II}, and A_k versus rain rate and frequency. These parameters in turn are determined by the propagation constants (a_I, ϕ_{If} etc.) corresponding to the raindrop symmetry axes. Nowland, et

al (1977) report the results of regression calculations performed in this manner for oblate spheroidal and Pruppacher-Pitter-form raindrops, for the Laws-and Parsons drop size distribution. More extensive results are included in CCIR Document 5/206 (1977), a Canadian submission to the Study Group 5 Final Meeting. That report also contains the regression coefficients for path length, u and v. These are given as functions of elevation angle for three ranges of rain rate, and were computed based on an empirical formula for path length.

The orientation distribution of the raindrops is the rain characteristic about which we know the least. It enters into the computation in finding a. and b. from a_1, a_2, b_1 and b_2, and in finding $\tilde{a}$. As stated earlier, it is apparently quite safe to ignore the effect of the angular distribution in the plane of incidence (see Figure 4.3-l). This allows us to set a = $90^o-\varepsilon$, the complement of the elevation angle of the path. The drop orientation angle θ with respect to the polarization direction, measured in the plane normal to the path, can be expressed as the difference $\theta = \phi-\tau$ where ϕ is the drop canting angle and τ is the polarization direction, both measured with respect to the horizontal. Since τ is known, it is the statistics of 0 that determines θ and σ_θ (or m_θ), i.e.

$$\bar{\theta} = \bar{\phi} - \tau, \quad \sigma_\theta = \sigma_\phi \tag{4.3-28}$$

It is convenient to describe the distribution of ϕ by an equivalent canting angle ϕ_e , defined by

$$\sin 2|\phi_e - \tau| = m_\theta \sin 2|\phi - 71 \tag{4.3-29}$$

The equivalent canting angle is the canting angle that identically oriented raindrops would need to have in order to produce the same XPD . Nowland, et al (1977) cite a measured value of 4° for ϕ_e that is consistent with independently-determined values of $\bar{\phi}$ and $\sigma\phi$, but give other experimental results that show little consistency. ϕ More work is clearly needed in characterizing the canting angle.

Chu (1980) employed a "two-tiered" Gaussian model for the canting angle. It assumes first that the instantaneous canting angle has a Gaussian distribution with mean ϕ_m and standard deviation S_ϕ. Second, the mean angle ϕ_m, which varies with time, is itself assumed to be Gaussian. The distribution of ϕ_m has zero mean and standard deviation S_m. The values of these parameters that apparently give the best agreement with experimental data are S_ϕ = 30° and S_m = 3°.

Based on this two-tiered model, Chu (1982) derived a semi-empirical formula for depolarization versus attenuation that agrees with experimental results over a wide range of frequency, polarization tilt angle and elevation angle. Cross-polarization discrimination for circular polarization XPD_c, in decibels, is given by

$$XPD_c = 11.5 + 20 \log f - 20 \log (CPA) - 40 \log (\cos\varepsilon) \quad (4.3\text{-}30)$$

where f is frequency in gigahertz, CPA is copolar attenuation in decibels, and ε is elevation angle. The formula for cross-polarization discrimination with linear polarization, XPD_L, in decibels, is

$$XPD_L = 11.5 + 20 \log f - 20 \log (CPA) - 40 \log (\cos\varepsilon) - 10 \log (1/2)(1 - 0.978 \cos 4\tau) - 0.075 (CPA) \cos^2\varepsilon \cos 2\tau \quad (4.3\text{-}31)$$

where τ is the polarization tilt angle measured from the horizontal.

Note that the formulas (4.3-30) and (4.3-31) contain a frequency dependence of 20 log f. This disagrees with the provisional formula of the CCIR (Equation 4.3-27), which has a 30 log f frequency dependence. There is little discrepancy between the predictions

given by the two formulas for frequencies in the vicinity of 12 GHz, but the above formulas give better agreement with data at 19 and 28 GHz .

4.3.3 Statistical Characteristics of Rain Depolarization

Two models have been proposed for predicting the statistical characteristics of rain depolarization. Chu (1980) determined functional dependencies of cross polarization on frequency, polarization and elevation angle, and presented techniques for finding depolarization statistics on the basis of rain rate or rain attenuation statistics. Kanellopoulos and Clarke (1981) developed a method of predicting long-term rain depolarization statistics on short terrestrial links. The distribution of cross-polarization isolation, in decibels, turns out to be approximately Gaussian. An assumption of uniform rain rate restricts the model to short paths, but an extension to the more general case of varying rain rate along the path is in progress. The general method should also be applicable to satellite paths.

Experimental depolarization data on satellite paths appears to be approximately normally distributed. Combining this with the observed log-normal distribution of rain attenuation, a probabilistic model of depolarization in combination with attenuation has been proposed (Wallace - 1981). In this model the joint probability density of XPD, in decibels, and the logarithm of rain attenuation, in decibels, is approximated by a bivariate Gaussian density. This description agrees fairly well with experimental results. The proposed model has been used in the analysis of single-site and diversity system availability.

4.3.4 Experimental Depolarization Data

The most extensive experimental investigations of depolarization above 10 GHz to date have been performed at Virginia Polytechnic Institute and State University (VPI & SU) at Blacksburg (Bostian and Dent - 1979) (Stutzman et.al. - 1983), the University of Texas (UT)

at Austin (Vogel - 1978), and the Bell Telephone Laboratories (BTL) in Holmdel, and Crawford Hill, N.J. (Arnold, et al - 1979). The signal sources for depolarization measurements conducted at these facilities have been beacons on the following spacecraft.

ATS-6	20 GHz, 30 GHz, LP
CTS	11.7 GHz, RHCP
COMSTAR	19.04 GHz, Vert. & Horiz. LP
COMSTAR	28.56 GHz, Vert. LP
SIRIO	11.6 GHz, RHCP

Four COMSTAR spacecraft, D-1 through D-4, have been used.

In the experiments, the signal levels in the copolarized and cross polarized channels were measured, either continuously or during periods of rain. The measurement records were typically used to generate XPD and CPA statistics and plots of XPD versus CPA. Some results of these experiments are presented in section 6.7.2.

Both the VPI and SU and the UT data bases have been processed to give XPD vs CPA on an instantaneous basis, and on a statistical basis. In the former case, XPD values that were observed at the same time as the corresponding CPA value are plotted. In the latter case, the XPD value that was not exceeded for a particular percentage of time is plotted against the CPA value that was exceeded for the same time percentage. An instantaneous XPD vs CPA plot was prepared for each month, and a curve of the form $XPD = \tilde{a} - \tilde{b} \log CPA$ was fitted to it. Table 6.7-1 shows the $\tilde{a}$ and $\tilde{b}$ parameters giving the best fit for each monthly plot for the 1978 VPI and SU data. The parameter R, which indicates how well the data fits the analytical curve ($R^2 = 1$ for perfect fit), is given for each case. The best-fit $\tilde{a}$ and $\tilde{b}$ values are quite variable month-to-month, and some months have very low R^2 values. The UT data gave similar results. This indicates that the formula is probably not very reliable for predicting XPD versus CPA on an instananeous basis. Statistical plots, on the other hand, generally show very

good fit to the formula. The VPI and SU CTS data (11.7 GHz) for the 1978 calendar year yielded $\tilde{a}$ - 41 dB and $\tilde{b}$ - 23.2 with R^2 = 0.95 when all data for CPA < 5dB is ignored. The UT data, covering about 18 months, gave $\tilde{a}$ = 41 dB, $\tilde{b}$ = 20.6 with R^2 = 0.99.

Figure 6.7-3 shows how the experimentally determined values of a and b for various frequencies and polarizations compare with the theoretically determined values from the formulas given previously. The theoretical predictions in general overestimate the depolarizing effects of the rain.

In the BTL experiment, co- and crosspolarized signal phase as well as amplitude was measured. This allowed the investigators to calculate XPD for arbitrary polarization states by vector manipulations. The beacon signal used, from a COMSTAR satellite, was linear polarized and oriented at about 21° from the local horizontal. Through the data conversion process, XPD versus CPA was determined on a statistical basis for linear polarization oriented 0°, 45° and 90° from horizontal, and RHCP. Figure 4.3-5 shows the median 19 GHz curves for the true polarizations (21° from vertical and horizontal) and for vertical, horizontal and 45°. The experiment confirmed the theoretical result that maximum XPD occurs at 45°. Also, the XPD values calculated for RHCP were virtually identical to those at 45°, which is predicted by theory. The figure shows that the 21° curves fall between the 45° and the vertical/horizontal curves, and that XPD for horizontal polarization is greater than for vertical polarization. Both of these results aqree with physical reasoninq。 A general aqreement with the XPD = $\tilde{a}$ - $\tilde{b}$ log CPA relation is evident for the lower three curves, in that they tend to lie near a straight line on the semilogarithmic plot. The CCIR approximation (4.3-27) is shown on the plot for the tilt angles 21° and 45°. In this case, the CCIR approximation appears to underestimate the depolarization.

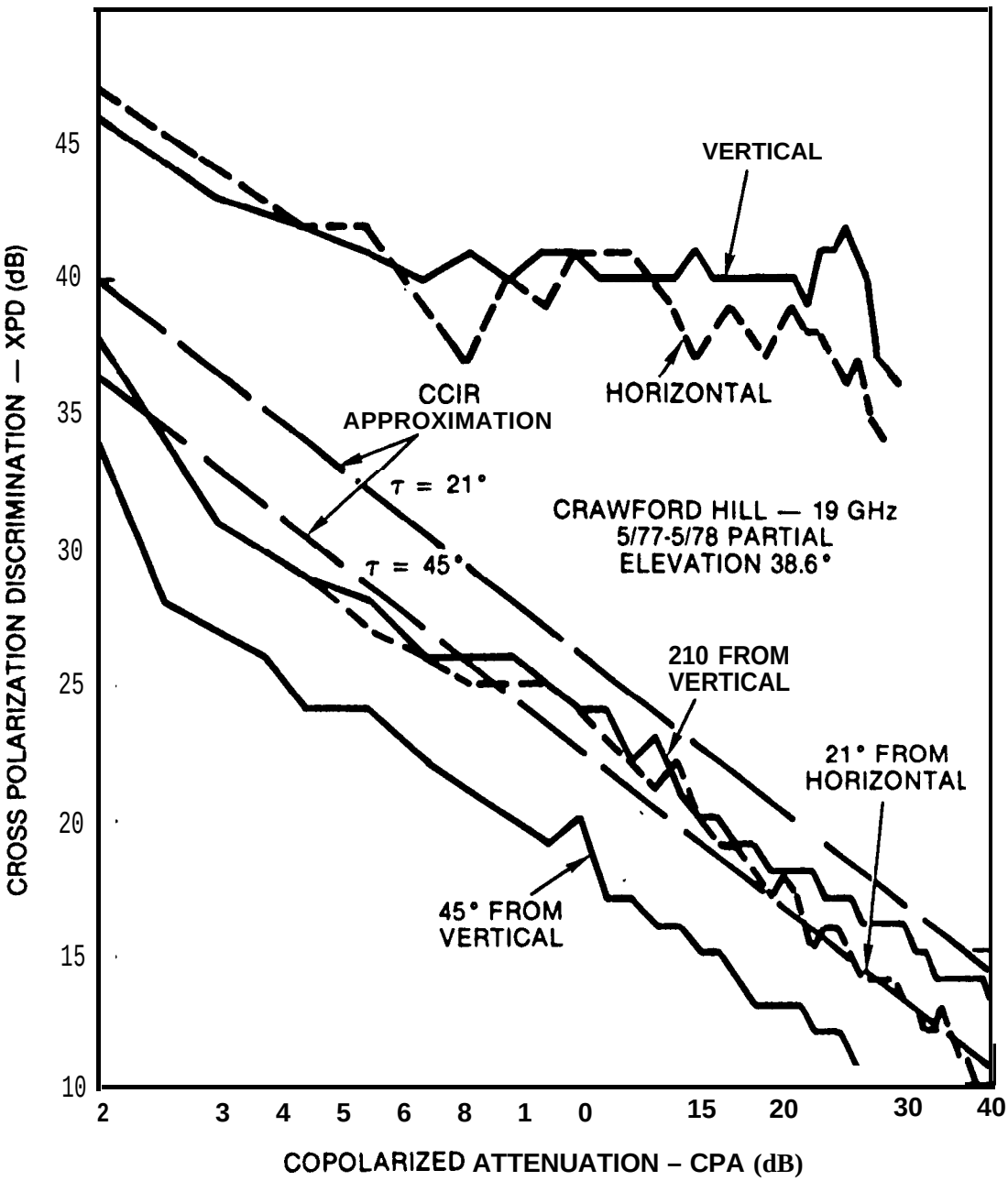

Figure 4.3-5. BTL COMSTAR Depolarization Experiment Results (Arnold, et.al. - 1979)

4.3.5 Phase of CrossPolarized Signal

Techniques have been developed for compensating for depolarization in dual-polarized satellite systems. They involve canceling the crosstalk in one channel by inserting a properly levelled and phased sample of the opposite channel's signal. The signal sample used for canceling must be exactly 180° out of phase from the crosspolarized signal for the technique to work. Its effectiveness depends, therefore on how well the control system can determine and track the phase of the crosspolarized signal. This is a function of variability and rate of change of that phase.

Estimating the performance of crosstalk cancellation systems is one motivation for investigating crosspolarized signal phase. Another reason is that the signal phase is sensitive to certain properties of the rain medium (e.g. canting angle), and its measurement can aid in modelling the propagation properties of rain phenomena.

Overstreet and Bostian (1978) at VPI and SU derived a theoretical description of the phase between the copolarized and crosspolarized signals when rain depolarization is present. They assumed identically oriented raindrops, canted at an angle θ with respect to a copolarized reference direction, having known differential attenuation and phase and a known effective path length. Using Chu's differential attenuation and phase values for the frequencies and elevation angles of the CTS and COMSTAR D-2 beacons, they predicted the phase as a function of θ and rain rate, then found phase versus the XPD value for the same rain rate. The path lengths used were derived from attenuation statistics for those beacons at the VPI and SU station. For linearly polarized signals at 11 and 28 GHz, it was found that the phase was a fairly weak function of XPD and t , typically remaining with a 45° sector for XPD values down to 15 dB *over* the expected range of θ. For circular polarization, it was found that the phase difference A_c is given by

$$\Delta_c = \pm 2\theta + \Delta\ell(\theta = 45°) \qquad (4.3\text{-}30)$$

where $\Delta\ell$ is the phase difference for LP waves, and the sign of the first term depends on whether RHCP or LHCP is copolarized. The LP phase difference at $\theta = 45°$ is only weakly dependent on XPD so the 2θ term predominates in AC.

Experimental data from the CP CTS beacon at 28.56 GHz generally confirmed the theoretical expectations. The phase difference of the LP signal normally remained in a 20-30° range during a rain depolarization event, whereas the CP signal phase difference varied widely during the course of a rain event. The phase versus XPD changes generally followed a characteristic sequence during convective storms. This indicated the changes in the nature of the depolarizing medium, primarily in predominant canting angle of the raindrops present, through the passage of the storm cell.

The experimental evidence suggests that crosstalk cancellation schemes would be more effective using LP than CP waves. The phase of the crosspolarized signal, which must be estimated by the cancellation system, is much less variable with linear polarization. In fact, setting the phase of the cancellation signal to a constant value would give a degree of effectiveness, while eliminating the need for a complex phase shifter control system.

4.3.6 Rate of Change of Depolarization

To more fully characterize depolarization, some quantitative description of the rate of change of the amplitude and phase of the crosspolarized signal would be desirable. This information would assist us in designing adaptive controls for crosstalk cancellation systems, and may also provide further insight into the nature of the meteorological process responsible for depolarization. However, there has apparently been little research effort expended to this end. Further experimental work, or further analysis of existing data bases, is needed in this area.

4.3.7 Rain Depolarization Dependence on Elevation Angle and Frequency

Knowledge of the dependence of crosspolarization discrimination on elevation angle and frequency is quite valuable because it allows us to extend the usefulness of time-consuming and costly measurements. Unfortunately, the present limited body of experimental evidence does not overwhelmingly support the theoretical scaling relations, so they must be used with caution.

The expression obtained earlier for XPD (eq. 4.3-16),

$$XPD = -20 \log\left[\frac{1}{2} m_\theta L |\Delta k'| \cos^2\varepsilon \sin 2\bar{\theta}\right] \qquad (4.3\text{-}31)$$

can be rewritten to explicitly show the elevation angle and frequency dependencies. For the CP case, corresponding to the minimum XPD, we have $\bar{\theta} = 45°$ which gives

$$\begin{aligned} XPD = & -20 \log (L \cos^2\varepsilon) \\ & -20 \log |\Delta k'| \\ & -20 \log (m_\theta/2) \end{aligned} \qquad (4.3\text{-}32)$$

Using the empirical relations (Nowland, et al-1977):

$$\begin{aligned} L &= [7.41 \times 10^{-3} R^{0.766} + (0{,}232 - 1.8 \times 10^{-3} R) \sin \varepsilon]^{-1} \\ |\Delta k'| &\cong c(f)\, R^{d(f)} \end{aligned} \qquad (4.3\text{-}33)$$

It is apparent that the first term in the XPD expression is a function of rain rate and elevation angle only, and the second term is a function of rain rate and frequency only. These terms are plotted in Figure 4.3-6. The last term can be considered constant, though it may also be a function of rain rate. For $m_\theta = 0.8$, the last term is 8 dB.

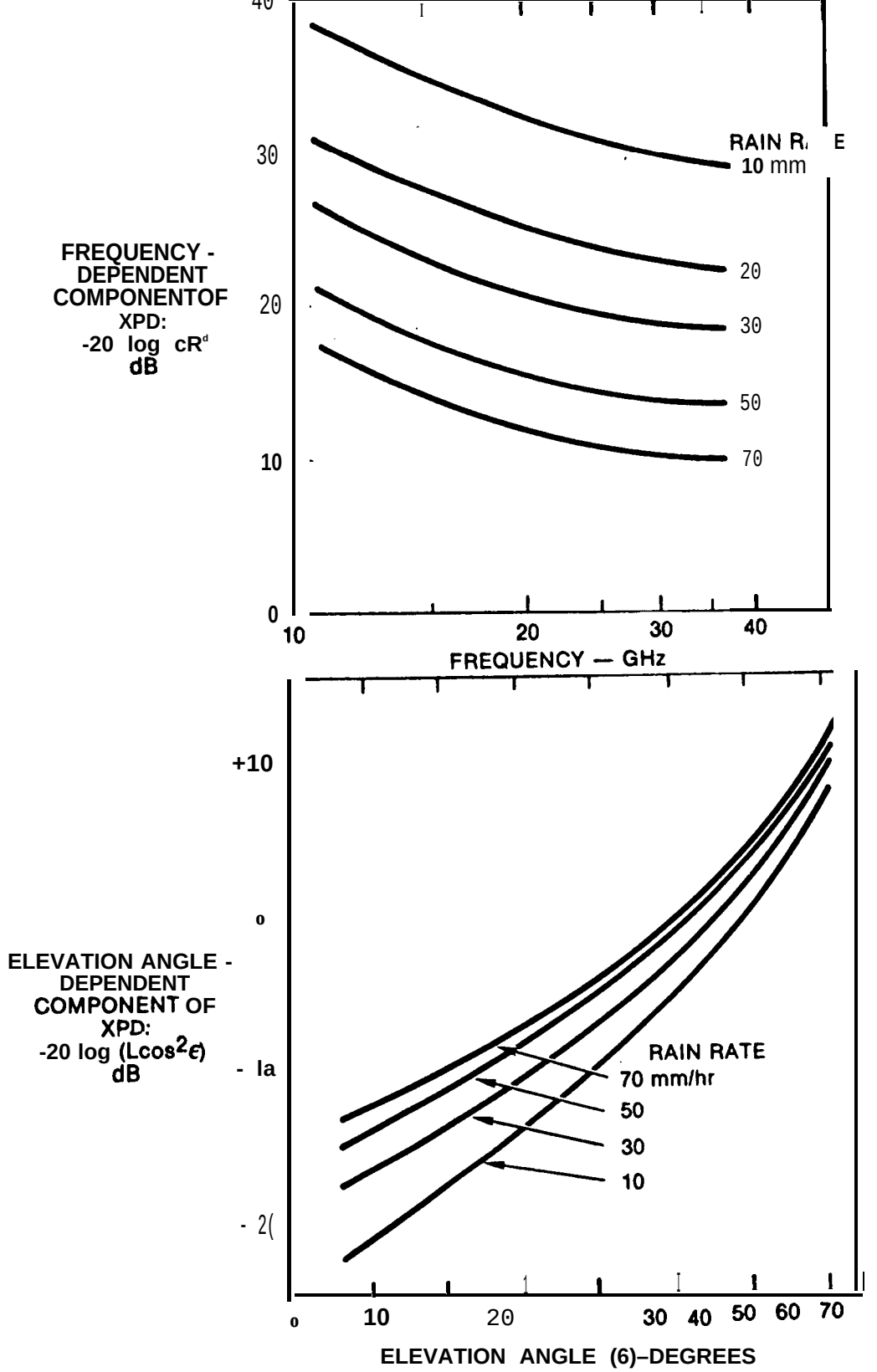

Figure 4.3-6. Frequency and Elevation Angle Dependence of. XPD for CP

Another depiction of the frequency dependence of XPD is shown in Figure 4.3-7. It shows the predicted XPD vs CPA relations for fixed frequencies and elevation angle. It is clear that, for any given rain rate, both CPA and XPD get worse as frequency increases. However, for a given value of CPA, XPD improves with frequency.

4.4 ICE DEPOLARIZATION

The second major cause of depolarization on Earth-space paths, besides rain, is the presence of ice crystals in clouds at high altitudes. Ice crystal depolarization is different from rain depolarization in that it is not accompanied by appreciable copolarized attenuation. This is because the depolarization is caused primarily by differential phase shifts, rather than differential attenuation, which is responsible for rain depolarization. Another distinguishing characteristic is that the amplitude and phase of the crosspolarized signal often undergo abrupt, coincident changes with large excursions.

4.4.1 Meteorological Presence of Ice

Clouds present above the freezing level consist, completely or in part, of ice crystals. Cirrus clouds, and the "anvil" that forms at the top of mature thunderstorms are all ice, and the upper parts of cumulonimbus clouds are predominately ice. The crystals that are present have one of two shapes determined by the temperature at the time of formation. Very cold temperatures, below about -25°C, favor the formation of needle-shaped crystals. Flat, plate-like crystals form in a moderately cold environment (-9° to -25°C). The dimensions of the crystals vary between about 0.1 and 1 mm.

Ice crystals form on dust particle nuclei in the atmosphere. The relative abundance of dust particles has been hypothesized as the reason for differences observed in ice depolarization at different locations. In maritime regions, the air contains relatively few dust particles compared with continental areas. As a result of this, maritime air tends to have fewer, but larger ice

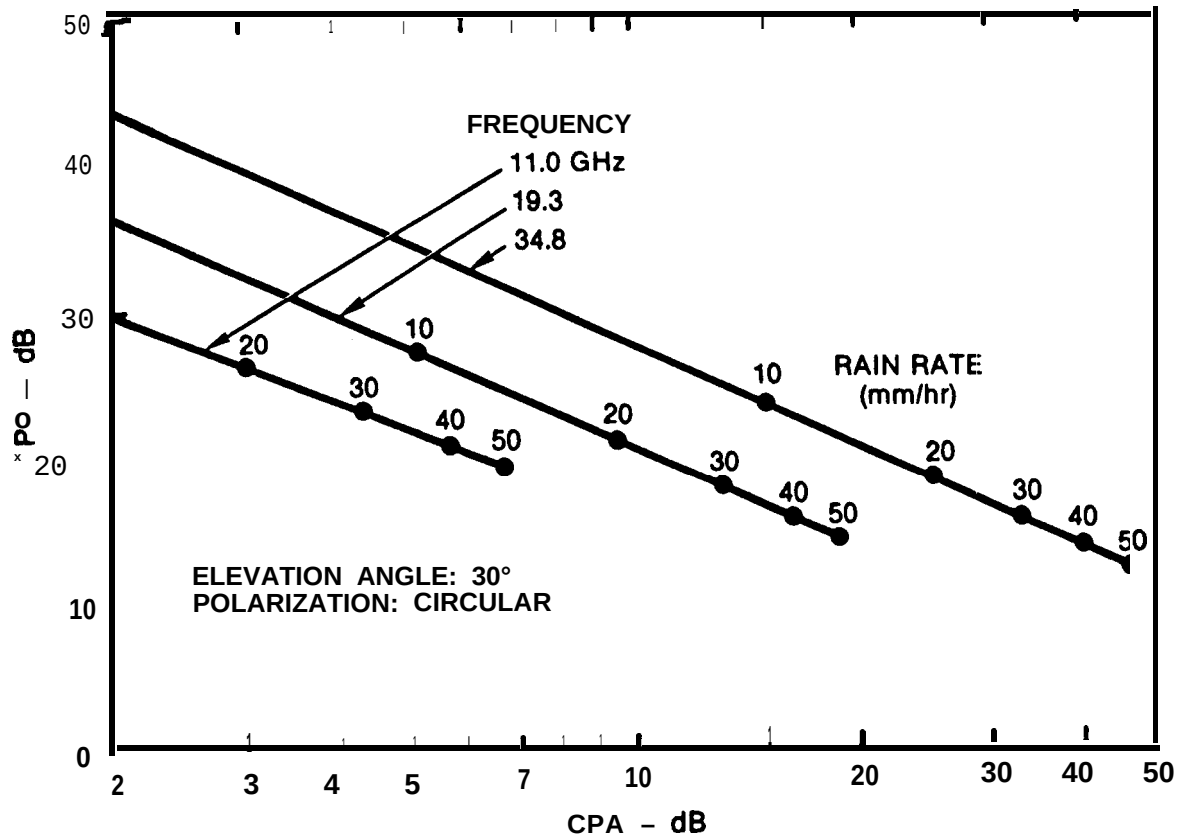

Figure 4.3-7. Frequency and Rain Rate Dependence of XPD and CPA

particles than continental air under similar conditions. It is believed that the presence of larger crystals accounts for the generally higher values of XPD observed in maritime versus inland locations (i.e., BTL versus VPI & SU).

Like raindrops, ice crystals are non-symmetrical and they have a dielectric constant much different from air. These are two of the necessary conditions for depolarization. A third condition, a preferred particle alignment, is also required. Oblate raindrops are aligned by aerodynamic forces, and their preferred alignment direction is affected by the prevailing winds. Aerodynamics also plays a role in aligning ice particles, but it is believed electrostatic forces also play a large part. This belief is supported by many observations during thunderstorms of rapid XPD changes coinciding with lightning flashes. This coincidence may be explained by the following: Electric fields present in regions between oppositely-charged clouds exert torques on the highly non-symmetrical ice crystals. When the field is sufficiently strong, these torques become significant in comparison with the turbulent aerodynamic forces, resulting in an average alignment of the "needle" crystal axes and the "plate" crystal planes along the direction of the field lines. When a lightning discharge takes place between the clouds, charges are equalized and the electric field intensity drops. Aeroydnamic forces then predominate, and the crystals quickly lose their preference for a particular direction of orientation (Bostian and Allnut - 1979).

4.4.2 Model for Ice Depolarization

Propagation through a region containing ice crystals can be analyzed in a manner analogous to that applied to rain. In the case of ice, the crystals are modelled as highly eccentric prolate spheroids ("needle" crystals) or oblate spheroids ("plate" crystals). Haworth, Watson and McEwan (1977) have performed this analysis. They assumed that due to aerodynamic forces, the "plate" crystals were oriented horizontally and the axes of the "needle" crystals stayed in the horizontal plane. Under this assumption, an

electrostatic field has no effect on "plates", and aligns the "needles" along the horizontal component of the field. Figure 4.4-1 shows the magnitude of the predicted ice XPD. The "needle''-produced XPD varies with ϕ, the average orientation angle of the crystal axes measured in the horizontal plane. The parameter a is a measure of the degree of alignment of the crystal axes. When the axes are uniformly distributed in all directions, a = 0, and when all crystals are oriented in the same direction, a = 1.

The phase of the crosspolarized signal, as predicted by the model, undergoes an abrupt change of 180° as ϕ passes through the values corresponding to the XPD peaks, (crosspolarized signal nulls). These are at 80° and 130° in the figure. When a is below some critical value, however, (falling between 0.5 and 1.0 for the example shown) the double null and accompanying phase jump don't occur. This phase reversal phenomenon has been observed at the time of lightning flashes in thunderstorms (see Figure 6.7-8) and is accompanied by a jump in XPD amplitude. Bearing the earlier discussion in mind, we would expect changes in a and ϕ to accompany lightning discharges. The same behavior has also been detected during the passage of non-electrically-active clouds (Shutie, et al-1978) . This implies that a particular mechanism, probably wind shear, is responsible for crystal alignment, besides electrostatic fields.

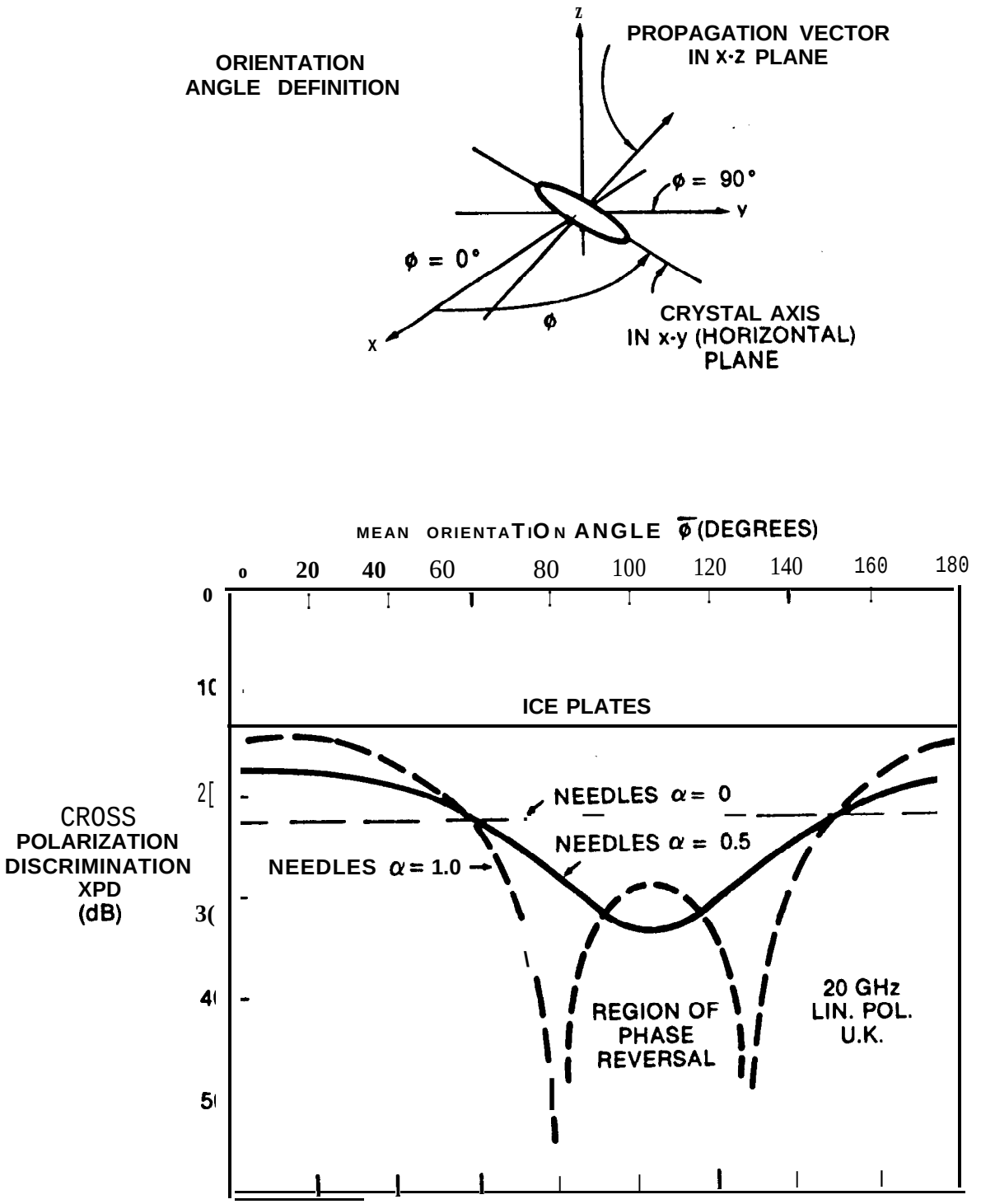

Figure 4.4-1. Definition of Orientation Angle φ and Predicted XPD (From Bostian and Allnut, 1979)

4.5 REFERENCES

Arnold, H.W. et al (1979), "Characteristics of Rain and Ice Depolarization for a 19 and 28 GHz Propagation Path from a Comstar Satellite," Record, Int'l Conf. on Communications.

Bostian, C.W. and J.E. Allnut (1979), "Ice-Crystal Depolarization on Satellite-Earth Microwave Radio Paths," Proc. IEE, Vol. 126, p. 951.

Bostian, C.W. and J.R. Dent (1979), "CTS 11.7 GHz Isolation Data for the Calendar Year 1978," VPI & SU Report, prepared for NASA under Contract No. NAS5-22577.

CCIR (1977), Document 5/206 (Canada), "Techniques for the Prediction of Rain Depolarization Statistics at Microwave and Millimeter Wavelengths."

CCIR (1978), "Propagation Data Required for Space Telecommunications Systems," Report 564-1, in Volume V, Recommendations and Reports of the CCIR - 1978, International Telecommunications Union, Geneva.

CCIR (1986), "Propagation Data and Prediction Methods Required for Space Telecommunications Systems," Report 564-3, in Volume V, Recommendations and Reports of the CCIR - 1986, International Telecommunications Union, Geneva.

Chu, T.S. (1974), "Rain-Induced Cross-Polarization at Centimeter and Millimeter Wavelengths," Bell Syst. Tech. Jrnl, Vol. 58, No. 8, pp. 1557 1579.

Chu, T.S. (1980), "Microwave Depolarization of an Earth-Space Path," BSTJ, Vol. 59, No. 6 (July-Aug) pp. 987-1107.

Chu, T.S. (1982), "A Semi-Empirical Formula for Microwave Depolarization Versus Rain Attenuation on Earth-Space Paths, "IEEE Trans. on Communications, Vol. COM-30, No. 12, (Dee) pp 2550-2554.

Haworth, D.P., P.A. Watson, and N.J. McEwan (1977), "Model for the Effects of Electric Fields on Satellite-Earth Microwave Radio Propagation," Elect. Letters, Vol. 13, p. 562.

Hendry, A., G.C. McCormick and B.L. Barge (1976), "Ku-Band and S-Band Observations of the Differential Propagation Constant in Snow," IEEE Trans. Ant. Prop., Vol. AP-24, No. 4, pp. 521-525.

Kanellopoulos, J.D. and R.H. Clarke (1981), "A Method of Calculating Rain Depolarization Distributions on Microwave Path," Radio Science, Vol. 16, No. 1 (Jan-Feb), pp. 55-65.

McCormick, G.C. and A. Hendry (1977), "Depolarization by Solid Hydrometeors," Electronics Letters, Vol. 13, No. 3.

Morrison, J.A., M.J. Cross, and T.S. Chu (1973), "Rain-Induced Differential Attenuation and Differential Phase Shift at Microwave Frequencies," BSTJ, Vol. 52, No. 4, pp. 599-604.

Nowland, W.L., R.L. Olsen, and I.P. Shkarofsky (1977), "Theoretical Relationship Between Rain Depolarization and Attenuation," Electronics Letters, Vol. 13, No. 22, pp. 676-677.

Oguchi, T. (1977), "Scattering Properties of Pruppacher-and-Pitter Form Raindrops and Cross Polarization Due to Rain: Calculations at 11, 13, 19.3 and 34.8 GHz," Radio Science, vol. 12, pp. 41-51.

Pruppacher, H.R. and R.L. Pitter (1971), "A Semi-empirical Determination of the Shape of Cloud and Rain Drops," J. Atmos. Science, Vol. 28, pp. 86-94.

Shutie, P.F., E.C. MacKenzie and J.E. Allnut (1978), "Relative phase Measurements at 30 GHz Between Copolar and Induced Crosspolar Signals Produced by Ice Particles on a Satellite-to-Ground Link," Elect. Letters, Vol. 14, No. 4, p.105.

Stutzman, W.L. (1977), "Mathematical Formulations and Definitions for Dual Polarized Reception of a Wave Passing Through a Depolarizing Medium (A Polarization Primer)," Virginia Polytechnic Institute & State Univ. Report, prepared under NASA Contract NAS5-22577.

Stutzman, W.L., C.W. Bostian, A. Tsolakis, and T. Pratt, (1983), "The Impact of Ice Along Satellite-to-Earth Paths on 11 GHz Depolarization Statistics," Radio *Science*, Vol. 18, No. 5, pp. 720-724.

Thomas, D.T. (1971), "Cross-Polarization Distortion in Microwave Radio Transmission Due to Rain," Radio Science, Vol. 6, No. 10, pp. 833-839.

Vogel, W.J. (1978), "CTS Attenuation and Cross-Polarization Measurements at 11.7 GHz," Final Report, Elect. Eng. Res. Lab., Univ. Texas at Austin, prepared under NASA Contract NAS5-22576.

Wallace, R.G. (1981), "Site Diversity Effects on Communication Satellite System Availability," ORI Technical Report 1891, prepared for NASA Headquarters under Contract NASW-3436.

Watson, P.A., and M. Arbabi (1973a), "Rainfall Crosspolarization at Microwave Frequencies," Proc. IEE, Vol. 120, No. 4, pp. 413-418.

Watson, P.A., and M. Arbabi (1973b), "Cross-Polarization Isolation and Discrimination," Electronics Letters, Vol. 9, N. 22, pp. 516-519.